Molecular Cell
Article

Functional Association of Gdown1 with RNA Polymerase II Poised on Human Genes

Bo Cheng,[1,6] Tiandao Li,[2,6] Peter B. Rahl,[3] Todd E. Adamson,[2] Nicholas B. Loudas,[2] Jiannan Guo,[2] Katayoun Varzavand,[2] Jeffrey J. Cooper,[2] Xiaopeng Hu,[4,5] Averell Gnatt,[4] Richard A. Young,[3] and David H. Price[1,2,*]
[1]Molecular and Cellular Biology Program
[2]Biochemistry Department
University of Iowa, Iowa City, IA 52242, USA
[3]Whitehead Institute for Biomedical Research, Cambridge, MA 02142, USA
[4]Department of Pharmacology and Experimental Therapeutics, University of Maryland School of Medicine, Baltimore, MD 21201, USA
[5]School of Pharmaceutical Sciences, Sun Yat-sen University, High Education Mega Center, Guangzhou, Guangdong 510006, China
[6]These authors contributed equally to this work
*Correspondence: david-price@uiowa.edu
DOI 10.1016/j.molcel.2011.10.022

SUMMARY

Most human genes are loaded with promoter-proximally paused RNA polymerase II (Pol II) molecules that are poised for release into productive elongation by P-TEFb. We present evidence that Gdown1, the product of the *POLR2M* gene that renders Pol II responsive to Mediator, is involved in Pol II elongation control. During in vitro transcription, Gdown1 specifically blocked elongation stimulation by TFIIF, inhibited the termination activity of TTF2, and influenced pausing factors NELF and DSIF, but did not affect the function of TFIIS or the mRNA capping enzyme. Without P-TEFb, Gdown1 led to the production of stably paused polymerases in the presence of nuclear extract. Supporting these mechanistic insights, ChIP-Seq demonstrated that Gdown1 mapped over essentially all poised polymerases across the human genome. Our results establish that Gdown1 stabilizes poised polymerases while maintaining their responsiveness to P-TEFb and suggest that Mediator overcomes a Gdown1-mediated block of initiation by allowing TFIIF function.

INTRODUCTION

Recent genome-wide analyses in which Pol II was mapped by ChIP-chip and ChIP-Seq demonstrated that promoter-proximal regions of most human genes and many *Drosophila* genes are loaded with polymerase and associated with histones containing the H3K4me3 mark associated with initiation (Gilchrist et al., 2008; Guenther et al., 2007; Hendrix et al., 2008; Muse et al., 2007; Nechaev and Adelman, 2011; Rahl et al., 2010; Zeitlinger et al., 2007). These findings are consistent with the polymerase being engaged in transcription and "poised" before entering productive elongation, and in fact, an engaged polymerase is found on most genes examined in detail (Lee et al., 2008; Peterlin and Price, 2006; Saunders et al., 2006). An early block to elongation was demonstrated originally for the human MYC gene, the HIV provirus, and *Drosophila* HSP70 gene and has since been found to be an important regulatory step in the expression of many specific genes (Boettiger and Levine, 2009; Core et al., 2008; Ni et al., 2008; Peterlin and Price, 2006; Romano and Giordano, 2008; Saunders et al., 2006; Zhou and Yik, 2006).

The positive transcription elongation factor, P-TEFb, is required to release the block to productive elongation (Marshall and Price, 1995), and a number of factors have been demonstrated to play both negative and positive roles in controlling elongation (Peterlin and Price, 2006; Saunders et al., 2006). Two negative elongation factors, DSIF and NELF, contribute to the block (Lee et al., 2008; Peterlin and Price, 2006), and P-TEFb reverses their effect and allows a high rate of elongation (Cheng and Price, 2007). Although progress has been made in understanding aspects of Pol II elongation control, the mechanisms employed to generate and regulate promoter-proximal polymerases are not fully understood.

Because of the prevalence of poised polymerases across the human genome and the likelihood that P-TEFb-mediated reversal of this block is key to regulating gene expression, we performed biochemical studies aimed at identifying the factor(s) involved in generating promoter-proximally paused polymerases. NELF and DSIF have a significant negative effect on the elongation properties of Pol II in a defined system, but a crude nuclear extract conferred even stronger negative properties to Pol II elongation complexes (Cheng and Price, 2007). In fact, crude extracts added back to isolated elongation complexes caused complete resistance to the strong positive effects of TFIIF on elongation (Cheng and Price, 2007). This result strongly suggests that additional factors work in concert with NELF and DSIF to modulate the properties of poised polymerases. In an attempt to identify the TFIIF resistance factor, a number of factors known to associate with Pol II were tested. In the present study we demonstrate that the TFIIF resistance activity is attributable to Gdown1, an Pol II binding protein that has been shown to be necessary for a Mediator-dependent response to activation of transcription in vitro (Hu et al., 2006). The work presented here suggests that Gdown1 provides a link between Mediator effects on initiation and regulation of transcription elongation.

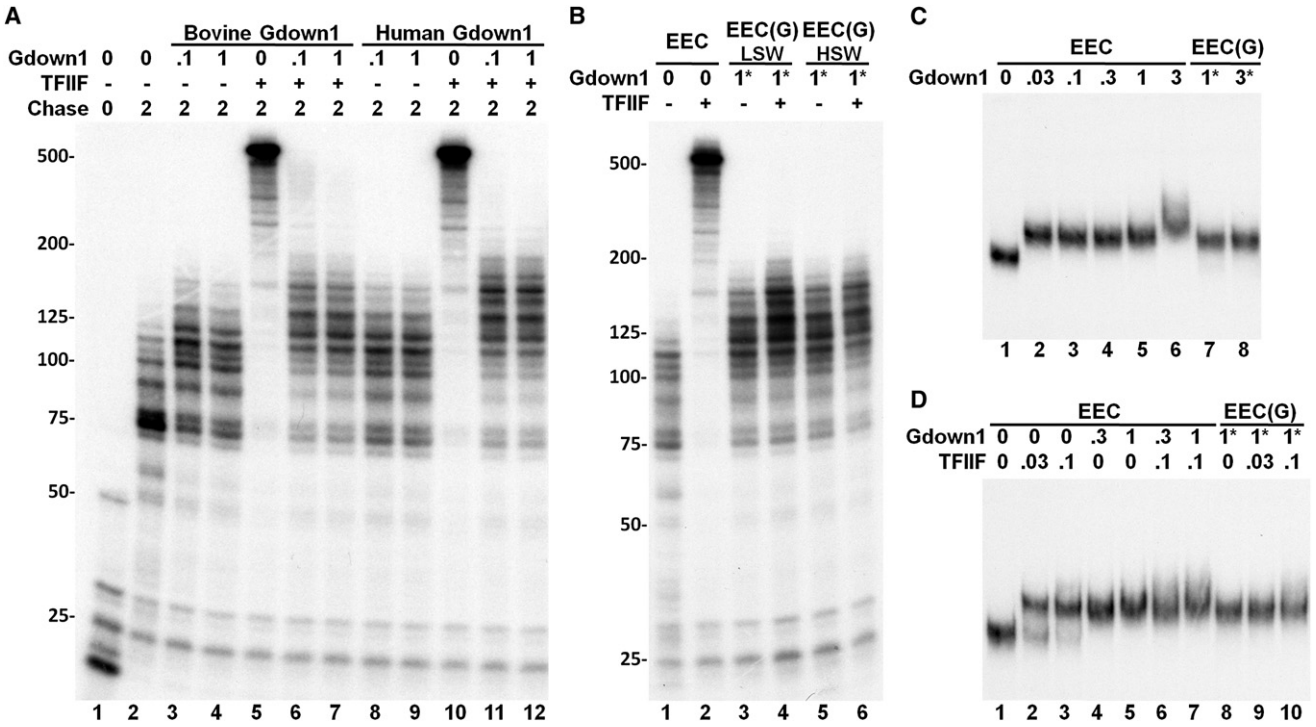

Figure 1. Gdown1 Inhibits the Function of TFIIF

(A) Isolated EECs were supplemented with indicated amounts of bovine or human Gdown1, and further elongation was performed for 2 min in the absence or presence of 0.1 pmole TFIIF. The autoradiograph shows labeled transcripts analyzed in a 6% TBE/urea gel.

(B) Isolated EECs were either left untreated or incubated with 1 pmole Gdown1 for 3 min at room temperature. After the incubation, the EEC(G)s were reisolated either with a low-salt wash (LSW) or with a high-salt wash (HSW) for 5 min. Then EECs or reisolated EEC(G)s were further elongated for 2 min in the absence or presence of 0.1 pmole TFIIF.

(C) Analysis of ECC•Gdown1 interaction using EC-EMSA. Isolated EECs were released from the beads through a restriction enzyme digestion and then incubated with indicated amounts of Gdown1. In lanes 7 and 8, EEC(G)s were formed, reisolated by a high-salt wash, and then released by a restriction enzyme digestion. The samples were then subjected to analysis on a native gel.

(D) EECs or EEC(G)s were incubated with the indicated factors and then analyzed by EC-EMSA. In lanes 6 and 7, TFIIF was added prior to the addition of Gdown1. Asterisks (*) in (B)–(D) signify that the indicated amounts of Gdown1 were incubated with EECs to form EEC(G) before reisolation.

RESULTS

Gdown1 Is the TFIIF Resistance Factor

To examine the effects of Gdown1, labeled elongation complexes were generated on an immobilized template containing the CMV promoter using a HeLa nuclear extract (HNE), and early elongation complexes (EECs) containing transcripts mostly less than 25 nt in length (Figure 1A, lane 1) were extensively washed with 1.6 M salt to strip off associated factors (Cheng and Price, 2007, 2009). The resulting EECs were assembled into reactions containing defined factors or crude extracts and then chased with physiological levels of NTPs (500 μM). The effects of elongation factors present during the chase are indicated by changes in the electrophoretic pattern of resulting transcripts.

When increasing amounts of either bovine (Hu et al., 2006) or human (see Figure S1 available online) recombinant Gdown1 were added to EECs, the factor had a small positive effect on elongation, evidenced by the increase in transcript length during a 2 min chase (Figure 1A). The two amounts of Gdown1 used correspond approximately to a 5-fold and 50-fold molar excess over the Pol II in the reactions, and correspondingly the elongation stimulation effect is saturated even at the lowest level. As expected, TFIIF alone dramatically increased the length of transcripts during the chase. Strikingly, Gdown1 from either species was able to inhibit the strong stimulatory effect of TFIIF (Figure 1A). We examined the association of Gdown1 with elongation complexes by incubating the factor with EECs and then washing the immobilized complexes with low (60 mM KCl) or high (1.6 M KCl) salt. Gdown1 bound very tightly, as evidenced by the slight positive effect on elongation following the washes and by the persistent resistance of these elongation complexes to TFIIF function (Figure 1B). These results strongly support the idea that Gdown1 is responsible for the TFIIF resistance activity previously described (Cheng and Price, 2007).

An elongation complex-electrophoretic mobility shift assay (EC-EMSA) (Cheng and Price, 2008) was performed to determine if Gdown1 inhibits TFIIF function by physically blocking TFIIF interaction with elongation complexes. EECs were liberated from the paramagnetic beads used to isolate them by restriction enzyme digestion of the DNA linking them to the beads and were then analyzed on a native gel using the short, labeled nascent

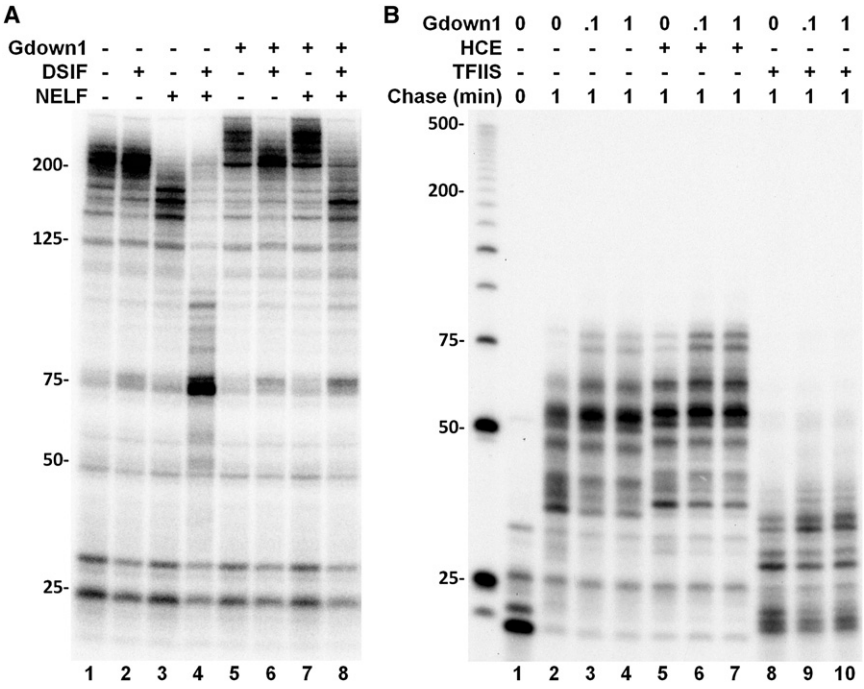

Figure 2. Gdown1 Affects the Functions of DSIF and NELF, but not HCE or TFIIS

(A) Isolated EECs or EEC(G)s (as described in the Figure 1 legend if Gdown1 is indicated) were supplemented with combinations of DSIF and NELF before a 6 min chase.

(B) Isolated EECs were supplemented with Gdown1, and further elongation was performed for 1 min in the absence or presence of 1 pmole HCE or TFIIS.

transcripts to detect the EECs. In the absence of other factors, the complexes have a unique mobility (Figure 1C, lane 1). Addition of increasing amounts of Gdown1 caused a reduction of mobility consistent with specific binding of Gdown1 to the elongation complexes (Figure 1C, lanes 2–6). Addition of 0.03 pmole of Gdown1 caused a complete shift, and only when 100 times more Gdown1 (3 pmole) was added was there any evidence of nonspecific binding (Figure 1C, lane 6). The specific shift, but not the nonspecific shift, was retained when the complexes were washed with 1.6 M KCl after factor binding (Figure 1C, lanes 7 and 8). TFIIF also caused a shift in the mobility of EECs, but the combination of TFIIF and Gdown1 resulted in only one shift (Figure 1D). EECs isolated after saturation with Gdown1 and a high-salt wash did not exhibit a second shift when TFIIF was added, strongly suggesting that Gdown1 blocks TFIIF binding (Figure 1D, lanes 8–10). Although it is possible that TFIIF displaced Gdown1 in the EC-EMSA, this would be contradictory to the finding that Gdown1 was stably bound and inhibited TFIIF in the elongation assay (Figures 1A and 1B). The results shown in Figure 1 are consistent with Gdown1 binding stably to Pol II elongation complexes and preventing the association and function of TFIIF.

Effect of Gdown1 on DSIF, NELF, HCE, and TFIIS

We next determined if Gdown1 would affect other factors known to functionally interact with elongation complexes. As a control, EECs without Gdown1 were isolated and chased for 6 min either alone or in the presence of DSIF, NELF, or both DSIF and NELF. DSIF had no effect; however, NELF displayed a moderate negative activity, and as seen before (Cheng and Price, 2007; Renner et al., 2001), the combination of DSIF and NELF was strongly negative. Different results were obtained with EECs that were converted into EEC(G)s by allowing Gdown1 to bind and then washing the excess away with 1.6 M salt as described in Figure 1B. On EEC(G)s, DSIF eliminated most of the positive effect of Gdown1 (Figure 2A, lane 6), and NELF had no effect (Figure 2A, lane 7). Together NELF and DSIF had a moderately negative activity on EEC(G)s. Gdown1 modulated the activities of DSIF and NELF individually and in combination with each other. The effect of Gdown1 on other Pol II-interacting factors, the human mRNA capping enzyme (HCE) and TFIIS, the transcript cleavage factor that can release Pol II blocked at arrest sites during elongation, was examined. The 5′ guanylylation of the RNA, evidenced by a shift of about 1.5 nt of transcripts longer than about 30 nt by HCE, or the negative effect exhibited by high concentrations of TFIIS (discussed more fully below), were unchanged by Gdown1 (Figure 2B). Also, neither HCE nor TFIIS affected the slight positive effect of Gdown1 (Figure 2B). These data demonstrate that Gdown1 does not directly interfere with the function of all Pol II binding factors, and this supports a dramatic role of Gdown1 in completely blocking TFIIF function and influencing both DSIF and NELF alone and in combination.

Function of Gdown1 in HeLa Nuclear Extract

To further characterize the properties of Gdown1, HNE was added to isolated EECs, and then elongation was carried out for 3 min in the presence of increasing amounts of Gdown1. When P-TEFb was functional, runoff transcripts were the predominant products generated (Figure 3A). Addition of Gdown1 had no effect on runoff at 0.1 pmole and only a slight negative effect at 1 pmole (Figure 3A, lanes 1–3). At the highest level of Gdown1, the slight loss of runoff transcripts was accompanied by an increase in short transcripts (Figure 3A, lanes 1–3). Inhibition of the P-TEFb by Flavopiridol (FP) (Chao and Price, 2001) revealed that Gdown1 blocked the appearance of the few remaining P-TEFb-independent runoff transcripts and led to an accumulation of transcripts between 20 and 75 nt in length (Figure 3A, lanes 4–6). The appearance of the very short transcripts in the absence of added Gdown1 can be explained by the presence of limiting amounts of Gdown1 in the HNE. We hypothesize that the crude extract contains factors that work with Gdown1 to generate a strong negative effect on elongation. In addition, our

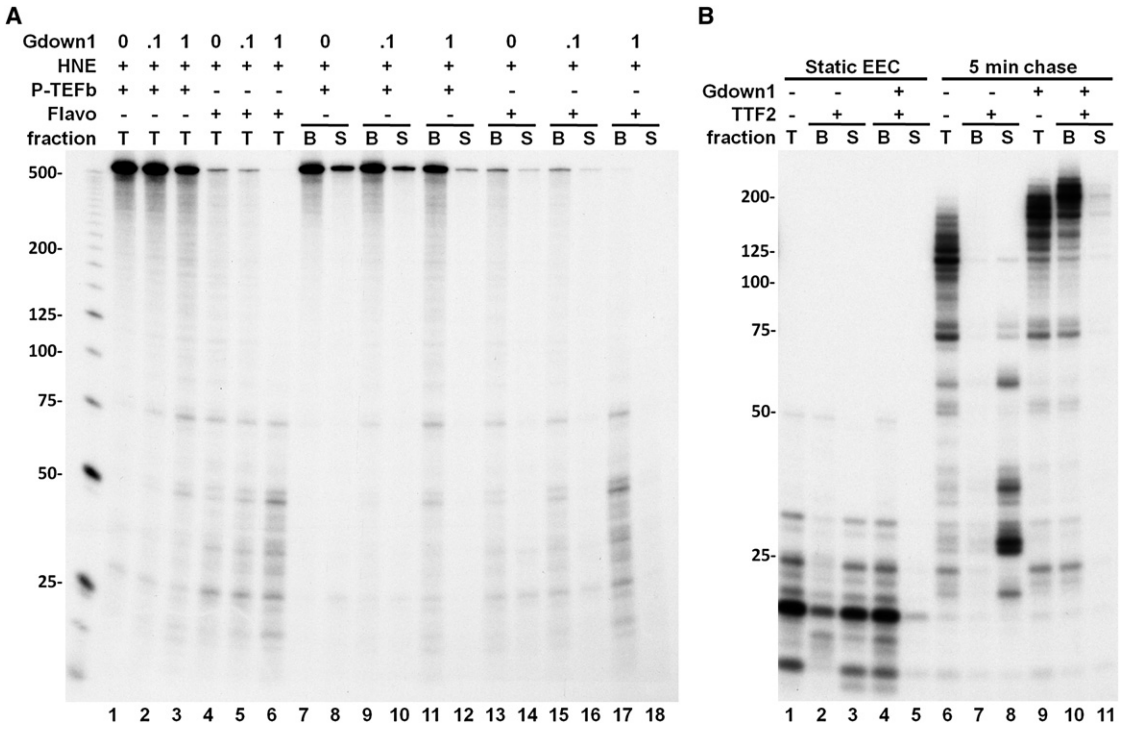

Figure 3. The Effects of Gdown1 on Pol II Elongation in the Presence of HNE

(A) Isolated EECs were supplemented with Gdown1, HNE, 1 pmole P-TEFb, or 1 μM FP as indicated, and further elongation was performed for 3 min. Transcription elongation was then stopped and an aliquot was taken from each reaction to show the pattern of transcripts for the total reaction ("T"). Another aliquot was separated into a supernatant fraction ("S") and a bead-bound fraction ("B").

(B) Isolated EECs were supplemented with 1 pmole Gdown1 and/or TTF2. Elongation complexes were either incubated with 0.5 mM ATP for 5 min at room temperature (lanes 1–5) or further elongated for 5 min upon the addition of 0.5 mM NTP (lanes 6–11). After the incubation or elongation reactions were done, the supernatant fractions in the indicated reactions were separated from the beads.

results indicate that P-TEFb is able to counteract Gdown1 and all negative factors.

To determine if Gdown1 enhanced termination in the presence of HNE, bead-bound elongation complexes (B) were separated from reaction supernatants (S) from an identical set of reactions (Figure 3A, lanes 7–18). As has been found before (Marshall and Price, 1992), some of the short transcripts were released from the template and appeared in the supernatant due to termination in the absence of extra added Gdown1. However, after Gdown1 was added, all transcripts remained bound to the template, indicating that termination was blocked. Because TTF2 is the major termination factor present in the extract (Jiang et al., 2004), we examined the effect of Gdown1 on TTF2 using the defined system with immobilized EECs. Gdown1 dramatically blocked the release of transcripts into the supernatant by TTF2 in the absence of elongation (Figure 3B, lanes 1–5) or during elongation (Figure 3B, lanes 6–11). These results indicate that Gdown1 renders the elongation complex resistant to TTF2.

Role of TFIIS in the Generation of Short Transcripts In Vitro

In an attempt to identify negative factors that worked with Gdown1 in HNE, extract was fractionated using phosphocellulose (P-11), Mono Q, Mono S, and glycerol gradient sedimentation. Using a variety of assays, four factors were identified. Representative assays and comparisons of the identified activities to known factors are shown in Figures S2 and S3. Importantly, both DSIF and NELF that were recently shown to comap with promoter-proximally paused Pol II (Gilchrist et al., 2008; Rahl et al., 2010) were rediscovered. One factor that that we call the Gdown1 negative accessory factor, GNAF, was detected, but the identity of that factor or factors was not determined because its activity was lost upon further fractionation. The final negative activity identified was the transcript cleavage factor TFIIS. Although TFIIS has been thought of as a "positive" factor, it does not increase the maximum rate of elongation by Pol II (Guo and Price, 1993; Luse et al., 2011), and its ability to stimulate the intrinsic transcript cleavage activity of Pol II is an inherently negative activity. At low concentrations its activity leads to suppression of pausing and arrest, but at higher concentrations normally found in HNE this activity has an overall negative effect on elongation (Figure S3C).

The function of TFIIS was examined by adding increasing amounts of the factor to EECs, EEC(G)s, EEC(G)s with DSIF and NELF, and EEC(G)s in the presence of HNE (Figure 4) and allowing elongation for 6 min. A strong negative effect was seen on EECs that saturated at the intermediate amount of TFIIS (Figure 4A, lanes 1–4). Except for the slight positive effect on elongation due to Gdown1, similar results were found when TFIIS was added to EEC(G)s (Figure 4A, lanes 5–8). Addition of DSIF

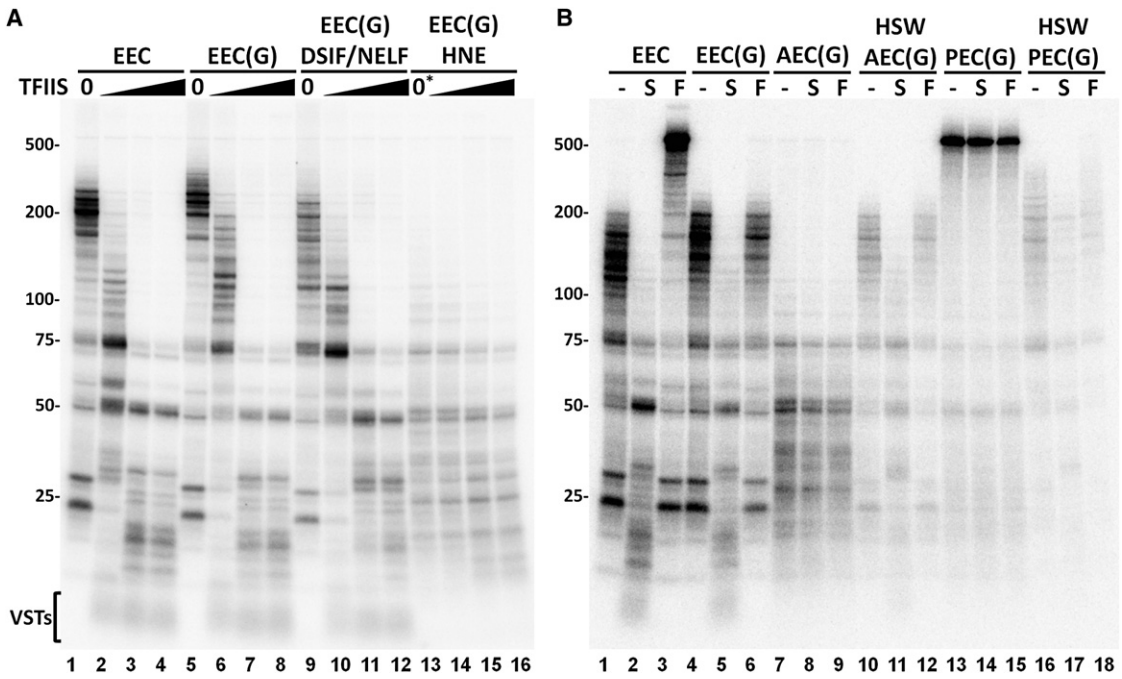

Figure 4. Negative Effect of TFIIS and the Influence of Other Factors on Gdown1

(A) EECs or EECs with Gdown1, EEC(G)s, were incubated with factors or extract and allowed to elongate for 6 min in the presence of increasing amounts of TFIIS (0, 0.5, 1.5, or 5 pmole).

(B) The effects of TFIIS (S) and TFIIF (F) were examined on the indicated elongation complexes. Elongation complexes were EECs or EEC(G)s. Abortive elongation complexes, AEC(G)s, are EEC(G)s in the presence of a HNE with FP. PECs are EEC(G)s incubated with HNE, extra P-TEFb, and ATP for 5 min and then chased in the presence of FP. Elongation complexes were washed with 1.6 M salt (HSW) before the chase. Chases were for 6 min and contained the indicated elongation complexes alone or were supplemented with TFIIS or TFIIF. Details are present in the Experimental Procedures and in the text. The asterisk above lane 13 in (A) signifies that although no TFIIS was added, the extract present does contain TFIIS.

and NELF had the expected negative effect on EEC(G)s, and TFIIS still acted as a negative factor (Figure 4A, lanes 9–12). Elongation of EEC(G)s in the presence of HNE without P-TEFb function gave only short transcripts, as expected. TFIIS had only a modest negative effect even at the highest levels (Figure 4A, lanes 13–16). This is likely due to the fact that TFIIS is present at high levels in the extract. The TFIIS-dependent, very short transcripts that appeared in all reactions without extract (Figure 4A, VSTs) were absent when extract was present. This could be due to a TFIIS-inhibitory activity present in the extract that works only on elongation complexes that have short transcripts or due to degradation of the very short transcripts that might be released from elongation complexes. Overall, these experiments and those shown earlier (see Figure 2B) suggest that TFIIS may play a role in promoter-proximal pausing and demonstrate that Gdown1 does not influence TFIIS activity.

Fate of Gdown1 during Productive Elongation

To determine what happens to Gdown1 during the P-TEFb-mediated transition into productive elongation, a variety of elongation complexes were tested for the retention of Gdown1 based on inhibition of TFIIF, but not TFIIS. On EECs devoid of Gdown1, TFIIS and TFIIF had strong negative and positive activities, respectively (Figure 4B, lanes 1–3). As demonstrated earlier, EEC(G)s responded only to TFIIS, not TFIIF (Figure 4B, lanes 4–6). Abortive elongation complexes (AECs) generated by incubating EEC(G)s in extract in which P-TEFb was inhibited did not respond to either TFIIS or TFIIF (Figure 4B, lanes 7–9). As before, the lack of response to TFIIS may be due to the fact that TFIIS is present in the extract and is functioning already. To determine if Gdown1 remained bound after incubation with extract, elongation complexes were washed with 1.6 M salt (HSW) to remove associated factors (but not Gdown1), and the resulting complexes were allowed to elongate. TFIIS, but not TFIIF, functioned on these complexes, indicating that, as expected, Gdown1 remained bound (Figure 4B, lanes 10–12).

Productive elongation complexes (PECs) can be made by incubating EECs and nuclear extract with P-TEFb and ATP for 5 min (Cheng and Price, 2007), and here PECs generated this way with EEC(G)s were able to reach runoff during a short chase. No effect was found when reactions containing PEC(G)s were supplemented with TFIIS or TFIIF during the chase (Figure 4B, lanes 13–15). Evidently, the P-TEFb-dependent transition into productive elongation makes elongation complexes resistant to the negative effect of TFIIS and causes them to exhibit properties similar to TFIIF stimulation. High-salt-washed PEC(G)s retained resistance to TFIIF, strongly suggesting that Gdown1 remained bound (Figure 4B, lanes 16–18). The slight lengthening of transcripts seen in these three lanes is due to limited elongation during the 5 min incubation with ATP due to the presence of

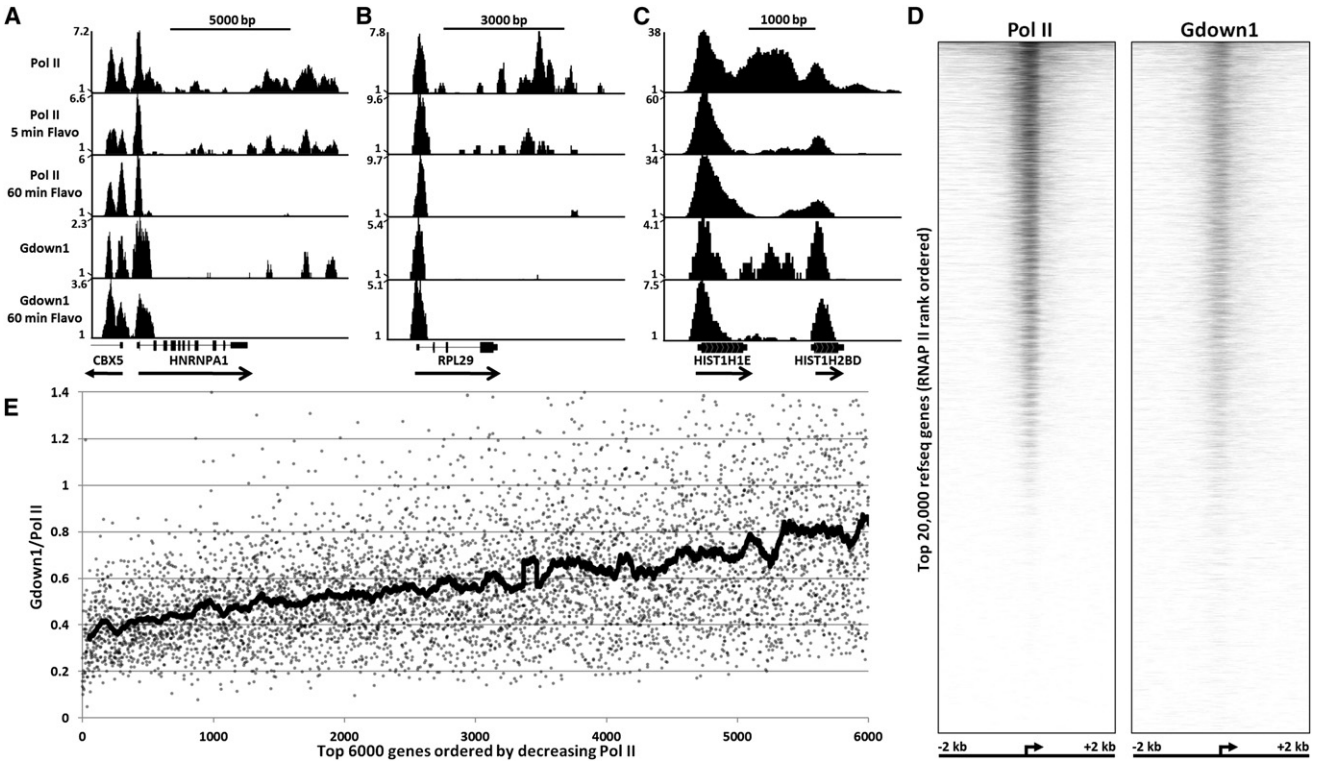

Figure 5. ChIP-Seq Analyses of Pol II and Gdown1

Pol II and Gdown1 occupancy in HeLa cells was determined by ChIP-Seq analysis as described in the Experimental Procedures. Vertical axis indicates occupancy normalized for the total number of reads obtained (counts per 1 million reads). (A)–(C) show density of Pol II and Gdown1 across indicated human genes. Pol II occupancy was determined in cells treated with FP for 0, 5, or 60 min. Gdown1 occupancy was determined in cells treated with FP for 0 or 60 min. (D) Shown is Pol II and Gdown1 binding from −2 kb to +2 kb around the TSS of top 20,000 RefSeq genes without TSSs within 1,000 bp of any other TSS, rank ordered from most Pol II bound to least Pol II bound. The high-resolution heat maps for Pol II and Gdown1 were generated as described in the Experimental Procedures. (E) Ratio of Gdown1 to Pol II for the region from −500 to +500 around the TSS of 5000 genes rank ordered by the amount of Pol II. Dots are individual ratios for each gene, and the thick line is a running average (100 points each).

low levels of NTPs in the extract. These results demonstrate that elongation complexes containing Gdown1 can enter productive elongation without loss of Gdown1.

Distribution of Pol II and Gdown1 across the Human Genome

The biochemical analyses described above provided mechanistic insights into the function of Gdown1 as a factor regulating the properties of poised polymerases, and because of this we reasoned that Gdown1 should be associated with poised polymerases in vivo. ChIP-Seq was used to map Gdown1 occupancy relative to Pol II in control HeLa cells or cells treated with FP. The following examples illustrate key aspects of what was found. In control cells, for the highly transcribed *HNRNPA1* gene there was a peak of Pol II density centered about 75 bp downstream of the annotated transcription start site (TSS), low levels of Pol II over the rest of the region encoding the mRNA, and high levels throughout an approximately 3 kbp region downstream of the poly(A) addition site (Figure 5A). After 5 min of FP treatment the only significant change in Pol II density was a loss of density in the region several kilobase pairs downstream of the large peak at the 5′ end of the gene. After 60 min of FP treatment, only Pol II over the 5′ end of the gene remained. Two peaks of such polymerases were found over the 5′ end of the *CBX5* gene (encoding HP1) that is transcribed in the opposite direction from *HNRNPA1* (Figure 5A). One of the peaks corresponds to a site 50 bp downstream of the annotated promoter, and the other is about 400 bp further downstream. EST data indicate that the second peak is likely generated by initiation from an unannotated promoter. Results similar to those found for *HNRNPA1* were found for the *RPL29* gene (Figure 5B). Interestingly, for histone genes, exemplified by *HIST1H1E*, in addition to a very strong peak of poised polymerases, a high density of Pol II was found downstream of the mature 3′ end even though different 3′ end processing machinery is used on histone mRNAs. Those polymerases terminated and were not replaced during a 5 min FP treatment, indicating that P-TEFb is needed for histone mRNA production and that termination occurs within 5 min. This quick turnover is probably due to the fact that the 3′ end polymerases are less than 1000 bp downstream of the TSS and because histone mRNA 3′ processing is rapid (Adamson and Price, 2003). Overall, the results from the control Pol II ChIP-Seq data set compared to two data sets from cells treated with FP for 5 or 60 min support the idea that P-TEFb is needed

for most mRNA production (Chao and Price, 2001; Rahl et al., 2010).

Because the in vitro evidence presented above strongly suggested that Gdown1 plays a role in the generation and stability of poised polymerases, we used an affinity-purified Gdown1 antibody (Figure S1) to map the genomic regions associated with Gdown1 using ChIP-Seq. As predicted, in both control and FP-treated HeLa cells, Gdown1 mapped over the promoter-proximally paused polymerases in all three examples shown (Figures 5A–5C). Gdown1 was found in the same region as 3′ Pol II on *HNRNPA1* and the *HIST1H1E* histone gene (Figures 5A and 5C); however, it was notably absent from that region on *RPL29* (Figure 5B). Variable amounts of Gdown1 were also found in regions occupied by promoter-proximally paused polymerase. An example of this is seen in the *HNRNPA1* gene that has two positions of poised polymerases with different Pol II occupancy (Figure 5A, 60 min FP treatment). The second smaller peak has about 80% less Pol II but an equal amount of Gdown1. Pol II binding was plotted from −2 kb to +2kb centered around the TSS for top 20,000 human RefSeq genes, rank ordered by the amount of Pol II detected in the region (Figure 5D). Gdown1 occupancy was plotted based on the Pol II rank order, demonstrating a strong spatial correlation between Gdown1 and Pol II occupancy at the 5′ end of most genes (Figure 5D). In this analysis, the intensity of Pol II gradually declined (as dictated by the rank ordering). The amount of Gdown1 also gradually declined for the bottom half of genes but was relatively constant over the top half of genes. The gene set in which all genes with TSSs within 1,000 bp of another were eliminated contains 20,286 genes. Of these, 9,366 have at least five sequences in the region from −500 to +500 for the control Pol II, and 92% of these also have at least five sequences from the control Gdown1 data set. To quantitatively assess the relative distribution of Pol II and Gdown1, the ChIP-Seq data were further analyzed by looking at the ratio of Gdown1 to Pol II on 1 kb regions centered on TSSs of the 6,000 genes with the highest levels of Pol II. Although a scatter plot of the data had a wide spread (Figure 5E, dots), a running average of the points showed a clear trend of increasing Gdown1 to Pol II ratio as the amount of polymerase decreased (Figure 5E, line). Both analyses suggest that Gdown1 is preferentially associated with promoter-proximally paused polymerases on genes with lower Pol II occupancy.

Metagene Analyses

To generate a more global view, the densities of Pol II and Gdown1 were compiled for the regions from −10,000 to +10,000 relative to the TSS of 20,286 RefSeq genes that do not have TSSs within 1,000 bp of another TSS. The signals from the lowest 10% of the 20,000 data points were averaged and subtracted from each point to remove the background, and then data sets were normalized so that the area under each distribution was equal (Figure S4 and Figure 6). This normalization appropriately emphasizes the positional information inherent in ChIP-Seq data and does not attempt to quantitatively compare data sets except for relative differences in positional information. Using these background subtracted and normalized data, the distribution of Pol II was found to peak about 45 bp downstream of the TSS with a shoulder centered about 250 bp upstream of the TSS and lower levels in the 2,000–10,000 bp region downstream of the TSS (Figure 6A). The shoulder likely represents divergent transcription, as has been recently described (Seila et al., 2009). Comparison with Pol II ChIP-Seq data from FP-treated cells demonstrated that the position of the peak of Pol II was shifted only a few bp downstream, and that as expected, transcription of far downstream regions was almost eliminated (Figure 6A). Interestingly, there was an increase in Pol II in the region from +300 to +1000 after FP treatment. These polymerases may have "crept" into this region during the hour without P-TEFb function. Identical analysis of Gdown1 data sets gave a slightly broader peak of Gdown1 around the TSS that included the upstream shoulder at −250 and the +300 to +1000 region just mentioned. Significantly, a downstream shift in the main peak to more closely align with the peak of Pol II occurred in the data from FP-treated cells (Figure 6B, center panel). The pattern for Gdown1 in the region downstream of the TSS was very similar to that seen with Pol II, including the reduction of signal in the region after FP treatment (Figure 6B, right). This supports the in vitro finding that Gdown1 is associated with Pol II and that a significant fraction of the PECs have Gdown1.

The effect of Gdown1 knockdown on the distribution of Pol II was examined next. Gdown1 is difficult to knock down due to toxic effects of reducing the protein. One siRNA was able to reduce the level of Gdown1 to about 20% after 2 days (Figure S1), and after 3 days there were fewer cells and those still contained about 20% of their normal level of Gdown1. Pol II ChIP-Seq from control and Gdown1 siRNA treated cells (48 hr) was performed and analyzed as above. Essentially no change was found in the position of the promoter-proximally paused polymerases (Figure 6C, center panel), but partial knockdown of Gdown1 caused an increase in polymerases downstream of the poised polymerases (Figure 6C, right panel). The significance of the change in downstream polymerases is indicated by the lack of a change in the upstream signals and from the fact that the Gdown1 siRNA curve did not cross the control siRNA curve in the 1,000–8,000 region (each of which is comprised of 7,000 data points). These results support a role for Gdown1 in helping to stabilize Pol II in promoter-proximal regions.

To follow up on the observation that the position of the peak of Gdown1 around the TSS shifted downstream after FP treatment of cells, a program was created to identify the precise position of peaks. The output of the program can be used to generate a track on the Genome Browser that displays both the size and the position of peaks. The FP-dependent downstream shift can be seen in the three examples in Figures 7A and 7B in which the program output is displayed over each track. While the peaks of Pol II remained relatively unchanged after FP treatment, the peaks of Gdown1 shifted downstream to more closely coincide with Pol II. A genome-wide average of the position (but not size) of peaks within 500 bp of the TSSs for Pol II and Gdown1 before and after treatment with FP was generated. Because information about peak height was not used, each gene is weighed equally in this average, instead of genes with the most Pol II or Gdown1 being overemphasized. The resulting distributions again demonstrated that the peak of Gdown1 but not Pol II shifted downstream after FP treatment (Figures 7C and 7D). To determine if the shift of Gdown1 was related to the relative expression of

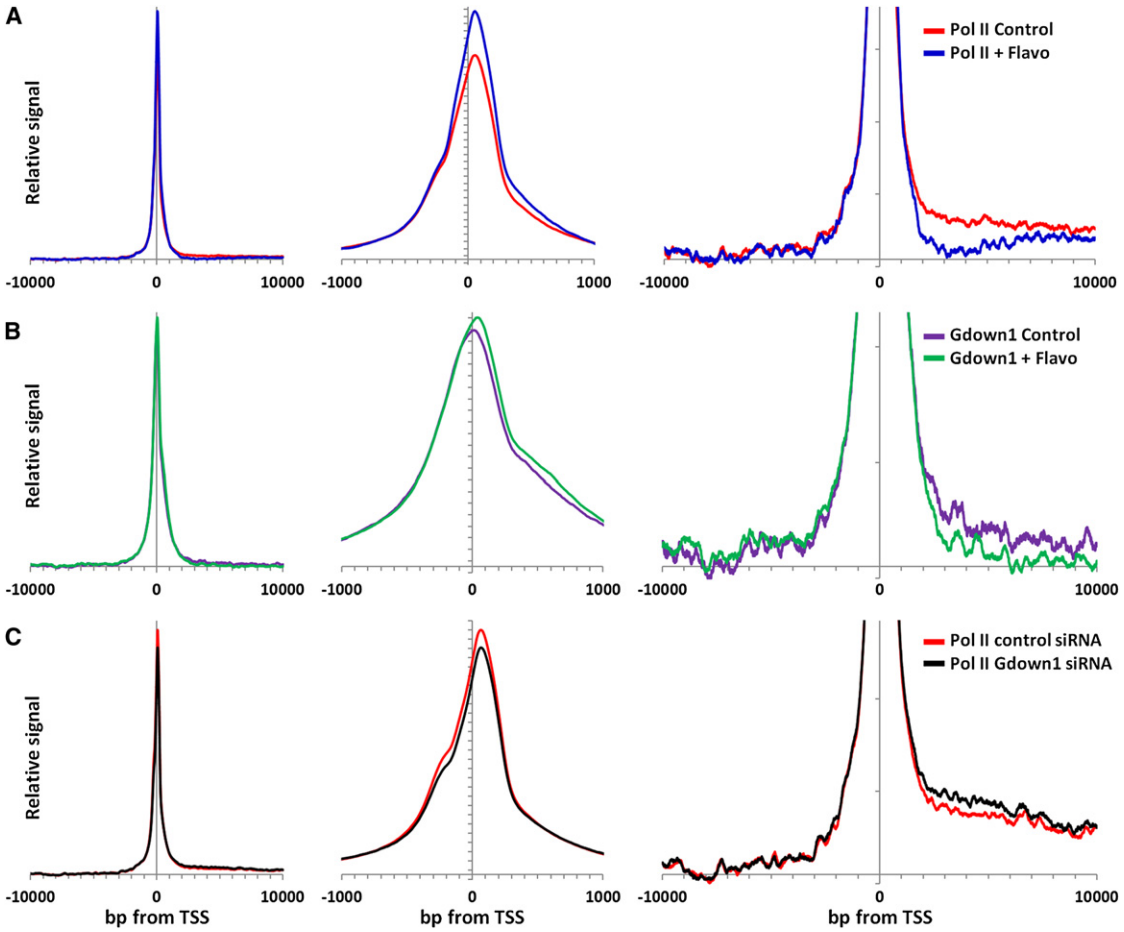

Figure 6. Global ChIP-Seq Analysis of Pol II and Gdown1

Average gene data for a customized set of 24,160 RefSeq genes, from which all genes with TSSs within 1,000 bp of each other have been excluded, were analyzed as described in the text and the Experimental Procedures. The three views depict relative signals in the indicated regions around the TSSs after averaging, background subtraction, and normalization of the entire −10,000 to +10,000 region (see Figure S4). The vertical scale in the right-hand panel was expanded 10-fold compared to other two panels.

(A) Indicated regions for Pol II from control (red) and FP-treated (blue) cells.

(B) Indicated regions for Gdown1 from control (purple) and FP-treated (green) cells.

(C) Indicated regions for Pol II from control siRNA (red) and Gdown1 siRNA-treated (black) cells.

genes, two sets of genes were compared. One contained the 200 most highly expressed genes based on RNA-Seq analysis of HeLa RNA, and the other was a group of 1,000 genes with lower levels of Pol II found in promoter regions. As expected, analysis of the first group showed a significant effect of FP, and the second had essentially no effect (Figure S5). Importantly, the shift of Gdown1 was more than double for the active genes (+45 bp) compared to the inactive genes (+20 bp) (Figure S5). Regardless of the method of analysis, it is clear, overall, that the position of Gdown1 shifts downstream to more closely coincide with the poised Pol II after treatment with FP, and this shift was most dramatic on genes that experience more productive elongation.

DISCUSSION

Our in vitro results using a defined transcription system provided strong evidence for the involvement of Gdown1 in the Pol II elongation control process. The striking set of properties demonstrated here for Gdown1 is not duplicated by any other known elongation factor. Interestingly, Gdown1 allowed a normal response to P-TEFb in the presence of HNE, but when P-TEFb was inhibited, the Gdown1-modified elongation complexes gave rise to only very short transcripts. The pattern of transcripts seen in the crude system without P-TEFb could be partially, but not completely, mimicked by the presence of only DSIF, NELF, and TFIIS. An extensive search for GNAFs yielded evidence for an additional GNAF that functions with NELF, DSIF, and TFIIS; however, we have been unable to purify it to homogeneity so far. Somewhat surprisingly, Gdown1 containing PECs maintained their resistance to the action of TFIIF and TTF2 in the presence of HNE. One of the most obvious characteristics of productive elongation is the high elongation rate achieved; therefore, resistance to TFIIF was not expected, because the factor is known to stimulate the elongation rate significantly

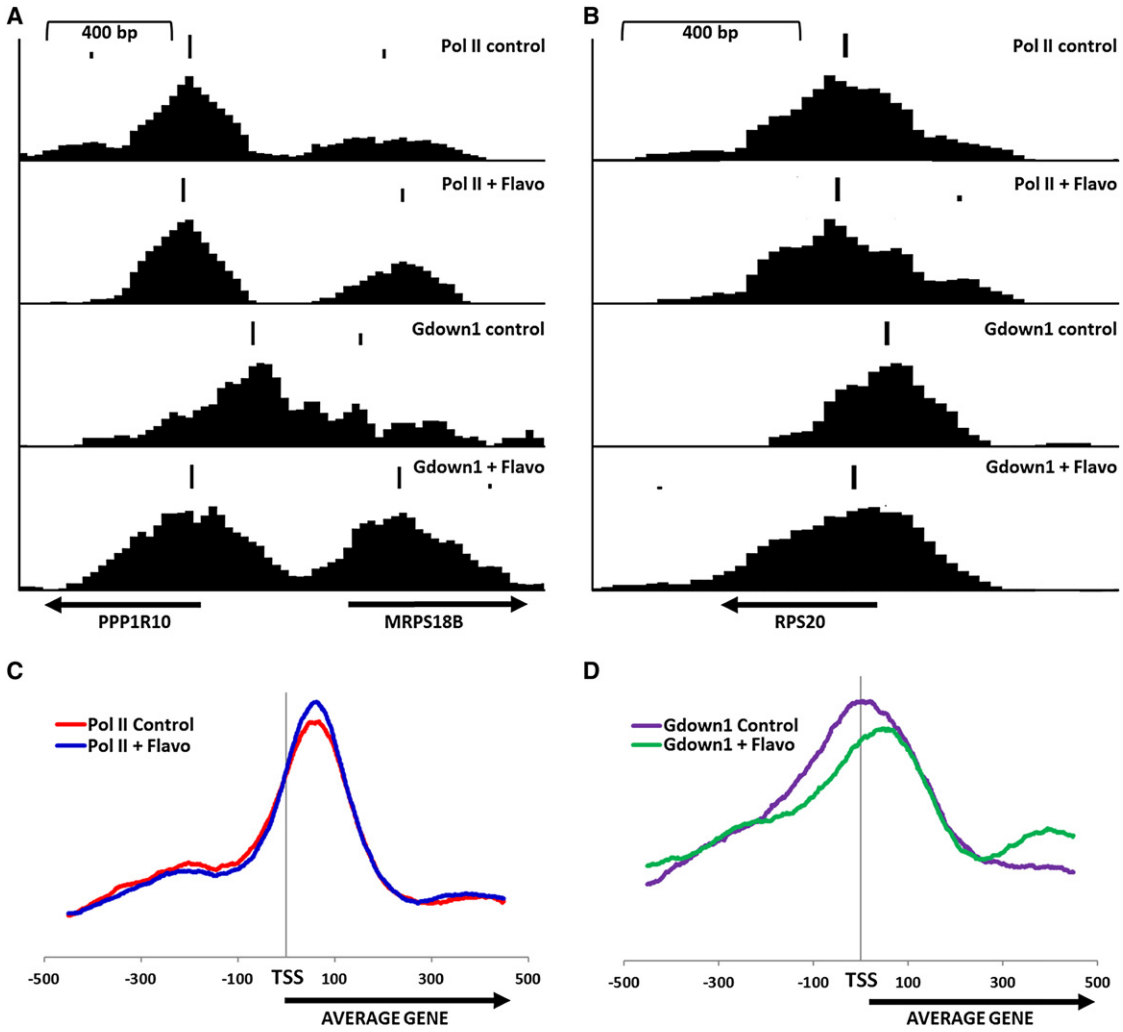

Figure 7. Effect of FP on Position of Gdown1

Peaks of Pol II and Gdown1 were identified using the program ChIP-Seq Peak and displayed above the individual tracks for Pol II and Gdown1 from control cells or FP-treated cells as indicated for the promoter regions of (A) PPP1R10 and MRPS18B and (B) RPS20. An average position for identified peaks for 25,530 RefSeq genes was compiled as described in the Experimental Procedures for (C) Pol II and (D) Gdown1 from control or FP-treated cells.

more than any other (Price et al., 1989). It is possible that this result was dependent on the exact conditions of the experiments performed. Further evidence for the role of TFIIF in productive elongation is needed. Most significantly, we showed here that when P-TEFb was inhibited the combination of Gdown1 with negative factors in HNE caused Pol II elongation complexes to become trapped on the template, unable to terminate.

Mapping of the location of Gdown1 across the human genome by ChIP-Seq provided additional strong evidence for a role of the factor in promoter-proximal pausing. Gdown1 mapped over essentially all poised polymerases, and while there was a general correlation of the amount of Gdown1 with the amount of Pol II, detailed analyses indicated that the ratio of Gdown1 to Pol II was not uniform for polymerases in different genes or for different polymerases in different regions of individual genes. The highest levels of Gdown1 relative to Pol II were found over poised polymerases on genes with relatively lower levels of Pol II occupancy, and these genes experienced less productive elongation. Dramatically differential loading (or removal) of Gdown1 was observed for many promoter-proximally paused polymerases close to each other on the same genes. A role for Gdown1 in stabilizing poised polymerases was supported by the finding that the highest concentrations of Gdown1 were found over those polymerases and from the finding that partial knockdown of Gdown1 led to an increase in downstream polymerases.

Our in vitro results suggest that promoter-proximally paused polymerases with Gdown1 associated may be relatively stably bound instead of constantly turning over. The lifetime of these polymerases cannot be measured in vivo using ChIP methods which just determine where polymerases are on average. However, the Lis lab has found using FRET that polymerases are stopped in vivo on the *Drosophila* HSP70 gene after induction, but in the absence of P-TEFb function are stable for up to the 3 min that are addressable by their assay (Ni et al., 2008). Our

results suggest that the dwell time of some poised polymerases may be significantly longer. For highly expressed genes, the dwell time is limited by the number of mRNAs produced per hour. For genes that are only rarely transcribed, the turnover of poised polymerases may only be limited by the occasional function of P-TEFb and in the extreme case by the cell cycle. For dividing cells, it is likely that replication fork movement is not compatible with stably poised polymerases. Also during mitosis, all polymerases terminate. Because TTF2 is responsible for termination during mitosis (Jiang et al., 2004) and it is inhibited by Gdown1, there must be a mechanism to reverse the effects of Gdown1 during mitosis.

The only other previous biochemical study of Gdown1 found that the protein was strongly associated with less than half of the Pol II purified from calf thymus and that transcription reactions reconstituted with the polymerase containing Gdown1 were dependent on Mediator to observe strong effects of activators (Hu et al., 2006). The authors concluded that Gdown1 played a negative role in transcription that was overcome by Mediator. The runoff assay used in that study required both initiation and elongation for a significant distance. However, because DSIF, NELF, TFIIS, and GNAF, as well as P-TEFb, were not present in their defined system, the inhibitory role of Gdown1 in that study was likely a negative effect on initiation. In support of this, we have observed that a titration of Gdown1 into HNE leads to a direct inhibition of initiation (data not shown). Our results demonstrate that Gdown1 blocks the binding of TFIIF and suggest that their results could be explained by Mediator-dependent removal or modification of Gdown1 that would allow TFIIF to bind and Pol II to initiate. A role for Gdown1 in regulating TFIIF binding to Pol II in the absence of nucleic acids is supported by EM structures of mammalian Pol II with either Gdown1 or the large subunit of TFIIF bound. In that study, part of the density of Gdown1 overlaps the binding site of TFIIF, providing a structural explanation for the exclusion of TFIIF by Gdown1 (Weihau Chang, personal communication).

A model can be created that is consistent with all of the information gathered to date on the function of Gdown1 (Figure S6). Because Gdown1 was found on 30% of the polymerases isolated from calf thymus and 50% of polymerases from pig liver (Hu et al., 2006), it is possible that transcription cycles can be started with either form. In the absence of Gdown1, Pol II forms a preinitiation complex (PIC) with TFIIF and rapidly initiates (Figure S6A). The EECs come under the control of DSIF, NELF, and TFIIS, which keeps the poised polymerase close to the promoter waiting for a short time for P-TEFb to trigger the transition into productive elongation. Poised polymerases in the absence of Gdown1 are transient, due to their ability to be terminated by TTF2 (Jiang et al., 2004; Marshall and Price, 1992). If a PIC forms with Pol II containing Gdown1, initiation is blocked (Figure S6B). Mediator is then needed to ''remodel'' Gdown1 so that TFIIF can bind and initiation can occur. The poised polymerases are now controlled by DSIF, NELF, TFIIS, Gdown1, and GNAF. These polymerases are still responsive to P-TEFb but differ from those lacking Gdown1 in that their elongation is more restricted and they are resistant to termination and, thereby, stably poised. Importantly, the model provides an explanation of why a downstream shift of Gdown1 in FP-treated cells is seen. Since it is likely that poised polymerases preclude formation of PICs due to promoter occlusion (Kornberg, 2007), in normal, untreated cells, loss of a poised polymerase to productive elongation would allow a new PIC to form. The steady-state density of Gdown1 over the promoter region that is observed in control cells could be due to new PICs, some of which could contain Gdown1. In FP-treated cells, the P-TEFb-dependent transition into productive elongation is blocked, and therefore PIC formation would be blocked and less Gdown1 would be found over the promoter. The only Gdown1 detected under this condition would be in the region of the poised polymerase, in the region centered 250 bp upstream of the TSS potentially from divergent transcription, and in the region 300–1000 bp downstream of the TSS, which is what was found. This model does not take into account the possibility that Gdown1 might be associated with factors other than Pol II (like Mediator). If this is the case, then the shift could be due to transfer of Gdown1 from other factors to Pol II, but it is not obvious how this could be affected by FP treatment.

Previous studies have elucidated many aspects of the function of TFIIS, and although most have emphasized the suppression of pause and arrest sites, the negative role of TFIIS demonstrated in this study is not contradictory. The ability of TFIIS to affect elongation is manifest through its ability to stimulate the intrinsic transcript cleavage activity of Pol II (Guo and Price, 1993; Izban and Luse, 1993; Reines, 1992). The structure of TFIIS bound to Pol II is known (Kettenberger et al., 2004), and recent structural work on the backtracked state demonstrates details of the TFIIS•Pol II•nascent RNA interactions found at pause and arrest sites (Cheung and Cramer, 2011). At low concentrations the inherently negative activity of TFIIS has the effect of giving paused and arrested polymerases a chance to encounter the block a number of times, and this increases the number of polymerase molecules that pass through the site, thereby providing an overall positive effect on the average elongation rate. Even at the optimal concentration, TFIIS does not increase the rate of elongation of the fastest moving polymerases (Guo and Price, 1993; Luse et al., 2011). As we have demonstrated here, at slightly higher concentrations TFIIS negatively impacts elongation. Both outcomes are derived from ability of TFIIS to stimulate transcript cleavage, and the only difference is the balance between the NTP-driven forward motion of the polymerase and transcript cleavage. Evidently, at higher concentrations, transcript cleavage dominates. Concerning Pol II elongation control, on the positive side, the stimulation of nascent transcript cleavage has been shown to aid restarting of paused polymerases in *Drosophila* (Adelman et al., 2005). Based on in vitro experiments, we hypothesize that TFIIS may also have a role in helping keep Pol II poised in promoter-proximal positions. Supporting a negative role of TFIIS in vivo, it was recently demonstrated using global RNA-Seq that short nascent transcripts were slightly extended in cells when TFIIS was knocked down (Nechaev et al., 2010).

We have presented strong evidence that incorporation of Gdown1 into elongation complexes generates significantly more stably poised Pol II molecules with properties in vitro that mimic poised polymerases in vivo. This could be one of the main reasons that Pol II is found promoter-proximally paused on the majority of mammalian genes regardless of the level of

expression of those genes. At genes for which expression is low due to lack of recruitment of P-TEFb, a high fraction of polymerases contain Gdown1. This could be due to the fact that those polymerases do not terminate and over time become predominant. The model for incorporation of Gdown1 into poised polymerases requires that Mediator be present at all genes with poised polymerases. Evidence for Mediator over the promoters (slightly upstream of the poised polymerase) can be easily found in the Mediator ChIP-Seq data sets obtained from mouse embryonic stem cells (Kagey et al., 2010). Both highly expressed genes and genes that are not highly expressed contain Mediator slightly upstream of the poised polymerase (Figure S7). Stably poised polymerases would help keep these promoters open. A role for Gdown1 in promoter-proximal pausing might explain why knockdown of NELF did not relieve all blocks in *Drosophila* (Gilchrist et al., 2008) or mouse (Rahl et al., 2010) if Gdown1 and GNAF functioned at least partly independently of NELF. Supporting a conserved role for Gdown1 in metazoans, potential Gdown1 homologs are present throughout vertebrates and in *Drosophila*. However, the genetic linkage of Gdown1 with a glutamate receptor like protein in humans (Roginski et al., 2004) is not conserved. One study has shown that DSIF is needed to observe effects of Mediator on activation of transcription in vitro (Malik et al., 2007), but details of the functional interactions between Mediator, Gdown1, GNAF, NELF, DSIF, TFIIS, and P-TEFb action remain to be elucidated.

EXPERIMENTAL PROCEDURES

More detailed procedures can be found in the Supplemental Information.

Materials

Preparation of HNE (Adamson et al., 2003) and purification of P-TEFb (Cheng and Price, 2007), DSIF (Renner et al., 2001), NELF (Renner et al., 2001), HCE (Moteki and Price, 2002), TFIIS (Palangat et al., 2005), and TFIIF (Peng et al., 1998) were as described earlier. Gdown1 antibodies were generated in sheep and affinity purified.

Expression and Purification of Gdown1 Proteins

Human and bovine Gdown1 expression plasmids were constructed using pET151 vector (Invitrogen), and the bovine protein was purified as described previously (Hu et al., 2006). The recombinant His-tagged human Gdown1 protein was expressed in *Escherichia coli* and purified on Ni-NTA resin (QIAGEN) as previously described (Byers et al., 2005) and Mono Q as detailed in the Supplemental Information. SDS PAGE and silver staining for one of the final eluted fractions are shown in Figure S1.

In Vitro Transcription Assays

The generation and isolation of EECs using immobilized templates and in vitro transcription assays were as described earlier (Cheng and Price, 2007, 2009). Basically, elongation complexes containing RNA mostly less than 25 nt in length were generated by initiation with a 30 s pulse at 500 μM A,U, and GTP and 1 μM ^{32}P-CTP. The elongation complexes were washed with 1.6 M salt and then chased with added factors and 500 μM NTPs. Except where indicated, bovine Gdown1 was used in add-back assays. Labeled transcripts were analyzed in denaturing RNA gels using autoradiography or phosphorimaging.

Termination assays of stalled or elongating complexes were accomplished by incubation with the indicated amount of TTF2 for 5 min in the presence of only 500 μM ATP or all NTPs. In both cases, the reactions were stopped by addition of EDTA, and then the reactions were magnetically separated into beads and supernatant fractions. Elongation complex electrophoretic mobility shift assays were carried out using the protocol described previously (Cheng and Price, 2008).

Chromatin Immunoprecipitation and Sequencing

Chromatin immunoprecipitation (ChIP) assays were performed using the protocol described by Lee et al. (Lee et al., 2006). HeLa cells were grown to 90% confluence and treated for 1 hr with FP (final concentration 1 μM with 0.1% DMSO) or 0.1% DMSO alone. For each immunoprecipitation, 5 × 10^7-1 × 10^8 cells were used. Cells were crosslinked with 1% paraformaldehyde for 15 min before being stopped with 125 mM glycine. Cells were washed twice with cold PBS and harvested by scraping. Cells for each immunoprecipitation were pelleted in PBS and incubated for 10 min each in 10 ml of lysis buffer 1 (50 mM HEPES-KOH [pH 7.5], 140 mM NaCl, 1 mM EDTA, 10% glycerol, 0.5% NP-40, and 0.25% Triton X-100), followed by 10 ml of lysis buffer 2 (10 mM Tris-HCl [pH 8.0], 100 mM NaCl, and 1 mM EDTA), and finally sonicated in lysis buffer 3 (10 mM Tris-HCl [pH 8.0], 100 mM NaCl, 1 mM EDTA, 0.1% sodium deoxycholate, and 0.5% sarkosyl) on ice using a Fisher Model 550 Sonic Dismembrator (Fisher Scientific) at a setting of 4 for 18 20 s pulses with 1 min rests between pulses. After sonication, 1/10 volume of 10% Triton X-100 was added, and then the samples were spun at 20,000 g for 10 min at 4°C.

For each immunoprecipitation, 100 μl of protein G Dynabeads (Invitrogen) were washed with block solution (0.5% BSA in 1× PBS) three times and resuspended in 250 μl block solution. The beads were incubated with 10 μg of Pol II (Santa Cruz, sc-899) or Gdown1 antibody at 4°C overnight. After three washes in block solution, the beads were incubated with the sonicated cell lysate at 4°C overnight. The beads were then washed four times with RIPA buffer (50 mM HEPES-KOH [pH 7.5], 100 mM NaCl, 1 mM EDTA, 500 mM LiCl, 1% [v/v] NP-40, 0.7% sodium deoxycholate), and once with a buffer containing TE and 50 mM NaCl. Immunocomplexes were eluted for 30 min at 65°C with elution buffer (1% SDS, 50 mM Tris-HCl [pH 8.0], 10 mM EDTA) and the eluted material incubated in Elution buffer overnight at 65°C. DNA fragments were size selected from an agarose gel, blunt-ended, ligated to the Solexa adaptors, and sequenced using the Illumina 1G Genome Analyzer as described previously (Barski et al., 2007; Rahl et al., 2010).

Data Analysis

Raw sequences generated from Illumina/Solexa sequencer were aligned using ELAND software to NCBI Build 36.1 (UCSC hg18) of the human genome. To illustrate the entire DNA fragment, the 3′ end of each read was extended 200 bp. The reference genome was partitioned into 25 bp bins, and the total reads (including partial reads) in each bin were summed and used to generate the visualization file in wiggle (WIG) format.

For Figures 5E, 6, and 7, a custom annotated RefSeq gene list was generated by merging the all TSSs for each gene that were within 500 bases of each other. Then genes with TSSs within 1,000 bp of another TSS (6% of the total number) were removed from the list. After extension of each sequence by 200 bases, the number of reads within 10,000 bases of the TSS of each gene in the custom gene list was tabulated. Similar analysis was applied to the location of the center of peaks generated from the peak-finding algorithm for the region within 500 bp relative to the TSS. Heat maps were generated using the program R (http://www.r-project.org/). Genes were rank ordered based on the sequence density for Pol II from −2K to +2K from the TSS. A peak-finding algorithm (ChIP-Seq Peak) was designed to determine precise position and height of each significant peak.

ACCESSION NUMBERS

The ChIP-Seq data sets are deposited in the Gene Expression Omnibus under accession number GSE32442.

SUPPLEMENTAL INFORMATION

Supplemental Information includes seven figures, Supplemental Experimental Procedures, and Supplemental References and can be found with this article online at doi:10.1016/j.molcel.2011.10.022.

ACKNOWLEDGMENTS

We wish to thank Peter Nagy, Lori Wallrath, Miles Pufall, and members of the Price, Young, and Gnatt labs for suggestions on the manuscript. We also thank R.G. Roeder for the initial suggestion that Gdown1 and TFIIF might compete for binding to Pol II. This work was supported by National Institutes of Health (NIH) grants GM35500 and AI074392 to D.H.P., National Human Genome Research Institute (NHGRI) grant HG002668-05 to R.A.Y., and NIH grant GM64474 to A.G.

Received: March 28, 2011
Revised: August 5, 2011
Accepted: October 20, 2011
Published online: January 12, 2012

REFERENCES

Adamson, T.E., and Price, D.H. (2003). Cotranscriptional processing of Drosophila histone mRNAs. Mol. Cell. Biol. *23*, 4046–4055.

Adamson, T.E., Shore, S.M., and Price, D.H. (2003). Analysis of RNA polymerase II elongation in vitro. Methods Enzymol. *371*, 264–275.

Adelman, K., Marr, M.T., Werner, J., Saunders, A., Ni, Z., Andrulis, E.D., and Lis, J.T. (2005). Efficient release from promoter-proximal stall sites requires transcript cleavage factor TFIIS. Mol. Cell *17*, 103–112.

Barski, A., Cuddapah, S., Cui, K., Roh, T.Y., Schones, D.E., Wang, Z., Wei, G., Chepelev, I., and Zhao, K. (2007). High-resolution profiling of histone methylations in the human genome. Cell *129*, 823–837.

Boettiger, A.N., and Levine, M. (2009). Synchronous and stochastic patterns of gene activation in the Drosophila embryo. Science *325*, 471–473.

Byers, S.A., Price, J.P., Cooper, J.J., Li, Q., and Price, D.H. (2005). HEXIM2, a HEXIM1-related protein, regulates positive transcription elongation factor b through association with 7SK. J. Biol. Chem. *280*, 16360–16367.

Chao, S.H., and Price, D.H. (2001). Flavopiridol inactivates P-TEFb and blocks most RNA polymerase II transcription in vivo. J. Biol. Chem. *276*, 31793–31799.

Cheng, B., and Price, D.H. (2007). Properties of RNA polymerase II elongation complexes before and after the P-TEFb-mediated transition into productive elongation. J. Biol. Chem. *282*, 21901–21912.

Cheng, B., and Price, D.H. (2008). Analysis of factor interactions with RNA polymerase II elongation complexes using a new electrophoretic mobility shift assay. Nucleic Acids Res. *36*, e135. 10.1093/nar/gkn630.

Cheng, B., and Price, D.H. (2009). Isolation and functional analysis of RNA polymerase II elongation complexes. Methods *48*, 346–352.

Cheung, A.C., and Cramer, P. (2011). Structural basis of RNA polymerase II backtracking, arrest and reactivation. Nature *471*, 249–253.

Core, L.J., Waterfall, J.J., and Lis, J.T. (2008). Nascent RNA sequencing reveals widespread pausing and divergent initiation at human promoters. Science *322*, 1845–1848.

Gilchrist, D.A., Nechaev, S., Lee, C., Ghosh, S.K., Collins, J.B., Li, L., Gilmour, D.S., and Adelman, K. (2008). NELF-mediated stalling of Pol II can enhance gene expression by blocking promoter-proximal nucleosome assembly. Genes Dev. *22*, 1921–1933.

Guenther, M.G., Levine, S.S., Boyer, L.A., Jaenisch, R., and Young, R.A. (2007). A chromatin landmark and transcription initiation at most promoters in human cells. Cell *130*, 77–88.

Guo, H., and Price, D.H. (1993). Mechanism of DmS-II-mediated pause suppression by Drosophila RNA polymerase II. J. Biol. Chem. *268*, 18762–18770.

Hendrix, D.A., Hong, J.W., Zeitlinger, J., Rokhsar, D.S., and Levine, M.S. (2008). Promoter elements associated with RNA Pol II stalling in the Drosophila embryo. Proc. Natl. Acad. Sci. USA *105*, 7762–7767.

Hu, X., Malik, S., Negroiu, C.C., Hubbard, K., Velalar, C.N., Hampton, B., Grosu, D., Catalano, J., Roeder, R.G., and Gnatt, A. (2006). A Mediator-responsive form of metazoan RNA polymerase II. Proc. Natl. Acad. Sci. USA *103*, 9506–9511.

Izban, M.G., and Luse, D.S. (1993). SII-facilitated transcript cleavage in RNA polymerase II complexes stalled early after initiation occurs in primarily dinucleotide increments. J. Biol. Chem. *268*, 12864–12873.

Jiang, Y., Liu, M., Spencer, C.A., and Price, D.H. (2004). Involvement of transcription termination factor 2 in mitotic repression of transcription elongation. Mol. Cell *14*, 375–385.

Kagey, M.H., Newman, J.J., Bilodeau, S., Zhan, Y., Orlando, D.A., van Berkum, N.L., Ebmeier, C.C., Goossens, J., Rahl, P.B., Levine, S.S., et al. (2010). Mediator and cohesin connect gene expression and chromatin architecture. Nature *467*, 430–435.

Kettenberger, H., Armache, K.J., and Cramer, P. (2004). Complete RNA polymerase II elongation complex structure and its interactions with NTP and TFIIS. Mol. Cell *16*, 955–965.

Kornberg, R.D. (2007). The molecular basis of eukaryotic transcription. Proc. Natl. Acad. Sci. USA *104*, 12955–12961.

Lee, T.I., Johnstone, S.E., and Young, R.A. (2006). Chromatin immunoprecipitation and microarray-based analysis of protein location. Nat. Protoc. *1*, 729–748.

Lee, C., Li, X., Hechmer, A., Eisen, M., Biggin, M.D., Venters, B.J., Jiang, C., Li, J., Pugh, B.F., and Gilmour, D.S. (2008). NELF and GAGA factor are linked to promoter-proximal pausing at many genes in Drosophila. Mol. Cell. Biol. *28*, 3290–3300.

Luse, D.S., Spangler, L.C., and Ujvari, A. (2011). Efficient and rapid nucleosome traversal by RNA polymerase II depends on a combination of transcript elongation factors. J. Biol. Chem. *286*, 6040–6048.

Malik, S., Barrero, M.J., and Jones, T. (2007). Identification of a regulator of transcription elongation as an accessory factor for the human Mediator coactivator. Proc. Natl. Acad. Sci. USA *104*, 6182–6187.

Marshall, N.F., and Price, D.H. (1992). Control of formation of two distinct classes of RNA polymerase II elongation complexes. Mol. Cell. Biol. *12*, 2078–2090.

Marshall, N.F., and Price, D.H. (1995). Purification of P-TEFb, a transcription factor required for the transition into productive elongation. J. Biol. Chem. *270*, 12335–12338.

Moteki, S., and Price, D. (2002). Functional coupling of capping and transcription of mRNA. Mol. Cell *10*, 599–609.

Muse, G.W., Gilchrist, D.A., Nechaev, S., Shah, R., Parker, J.S., Grissom, S.F., Zeitlinger, J., and Adelman, K. (2007). RNA polymerase is poised for activation across the genome. Nat. Genet. *39*, 1507–1511.

Nechaev, S., and Adelman, K. (2011). Pol II waiting in the starting gates: regulating the transition from transcription initiation into productive elongation. Biochim. Biophys. Acta *1809*, 34–45.

Nechaev, S., Fargo, D.C., dos Santos, G., Liu, L., Gao, Y., and Adelman, K. (2010). Global analysis of short RNAs reveals widespread promoter-proximal stalling and arrest of Pol II in Drosophila. Science *327*, 335–338.

Ni, Z., Saunders, A., Fuda, N.J., Yao, J., Suarez, J.R., Webb, W.W., and Lis, J.T. (2008). P-TEFb is critical for the maturation of RNA polymerase II into productive elongation in vivo. Mol. Cell. Biol. *28*, 1161–1170.

Palangat, M., Renner, D.B., Price, D.H., and Landick, R. (2005). A negative elongation factor for human RNA polymerase II inhibits the anti-arrest transcript-cleavage factor TFIIS. Proc. Natl. Acad. Sci. USA *102*, 15036–15041.

Peng, J., Liu, M., Marion, J., Zhu, Y., and Price, D.H. (1998). RNA polymerase II elongation control. Cold Spring Harb. Symp. Quant. Biol. *63*, 365–370.

Peterlin, B.M., and Price, D.H. (2006). Controlling the elongation phase of transcription with P-TEFb. Mol. Cell *23*, 297–305.

Price, D.H., Sluder, A.E., and Greenleaf, A.L. (1989). Dynamic interaction between a Drosophila transcription factor and RNA polymerase II. Mol. Cell. Biol. *9*, 1465–1475.

Rahl, P.B., Lin, C.Y., Seila, A.C., Flynn, R.A., McCuine, S., Burge, C.B., Sharp, P.A., and Young, R.A. (2010). c-Myc regulates transcriptional pause release. Cell *141*, 432–445.

Reines, D. (1992). Elongation factor-dependent transcript shortening by template-engaged RNA polymerase II. J. Biol. Chem. *267*, 3795–3800.

Renner, D.B., Yamaguchi, Y., Wada, T., Handa, H., and Price, D.H. (2001). A highly purified RNA polymerase II elongation control system. J. Biol. Chem. *276*, 42601–42609.

Roginski, R.S., Mohan Raj, B.K., Birditt, B., and Rowen, L. (2004). The human GRINL1A gene defines a complex transcription unit, an unusual form of gene organization in eukaryotes. Genomics *84*, 265–276.

Romano, G., and Giordano, A. (2008). Role of the cyclin-dependent kinase 9-related pathway in mammalian gene expression and human diseases. Cell Cycle *7*, 3664–3668.

Saunders, A., Core, L.J., and Lis, J.T. (2006). Breaking barriers to transcription elongation. Nat. Rev. Mol. Cell Biol. *7*, 557–567.

Seila, A.C., Core, L.J., Lis, J.T., and Sharp, P.A. (2009). Divergent transcription: a new feature of active promoters. Cell Cycle *8*, 2557–2564.

Zeitlinger, J., Stark, A., Kellis, M., Hong, J.W., Nechaev, S., Adelman, K., Levine, M., and Young, R.A. (2007). RNA polymerase stalling at developmental control genes in the Drosophila melanogaster embryo. Nat. Genet. *39*, 1512–1516.

Zhou, Q., and Yik, J.H. (2006). The Yin and Yang of P-TEFb regulation: implications for human immunodeficiency virus gene expression and global control of cell growth and differentiation. Microbiol. Mol. Biol. Rev. *70*, 646–659.

Molecular Cell, Volume *45*

Supplemental Information

Functional Association of Gdown1 with RNA Polymerase II Poised on Human Genes

Bo Cheng, Tiandao Li, Peter B. Rahl, Todd E. Adamson, Nicholas B. Loudas, Jiannan Guo, Katayoun Varzavand, Jeffrey J. Cooper, Xiaopeng Hu, Averell Gnatt, Richard A. Young, and David H. Price

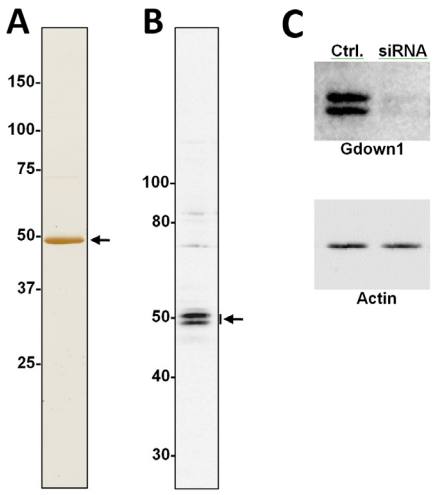

Figure S1. Recombinant human Gdown1, characterization of affinity purified Gdown1 antibody, and analysis of knockdown of Gdown1.

(**A**) Material eluted from the mono Q column used as the second step in purification of human Gdown1 expressed in *E. coli*. One of the mono Q fractions was analyzed by 6%-15% SDS PAGE and silver staining. The arrow points to the N-terminally His-tagged Gdown1. (**B**) Gdown1 antibodies were raised in a sheep (Elmira Biologicals) to the pure recombinant Gdown1 protein and were affinity purified as described in the Experimental Procedures section and used to probe a Western blot of a total HeLa cell lysate. (**C**) Knockdown of Gdown1 in HeLa cells. 48 hr after transfection with a control siRNA or Gdown1 siRNA cells were harvested and whole cell lysates were probed on a western blot for Gdown1 or actin as indicated. Knockdown was quantified from several loadings and it was determined that Gdown1 was reduced to 20% of that in control cells.

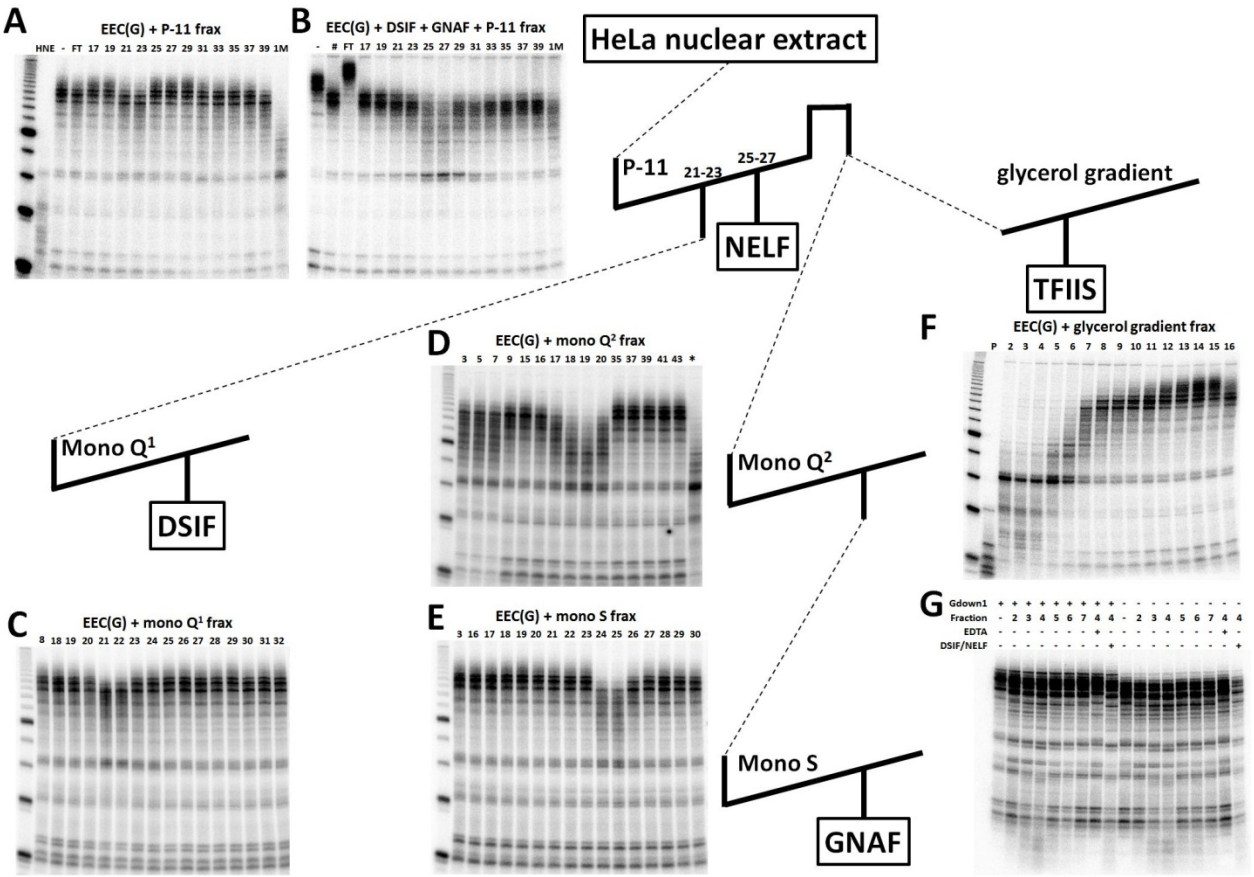

Figure S2. Fractionation of HNE to identify factors that contribute to the negative activity of Gdown1. A combination of phosphocellulose (P-11), Mono Q, Mono S ion exchange chromatography and glycerol gradient sedimentation was used to fractionate HeLa nuclear extract (HNE). Representative in vitro transcription assays containing the indicated factors and column fractions are shown. (**A**) and (**B**) assays across P-11 that detected DSIF and NELF. (**C**) Mono S column of P-11 fraction containing DSIF. (**D**) and (**E**) assays across Mono Q and Mono S of the 500 mM step fraction from P-11. This Gdown1 negative accessory factor (GNAF) does not correlate with any known elongation factor and was lost on subsequent attempts at purification. (**F**) and (**G**) assays of glycerol gradient fractions of the 500 mM step fraction from P-11. The first is an elongation assay showing the negative effect of the factor and the second is an assay in which elongation complexes were chased and reisolated and then subjected to backup reactions in the absence of NTPs. The negative activity correlated with magnesium dependent transcript shortening indicative of TFIIS.

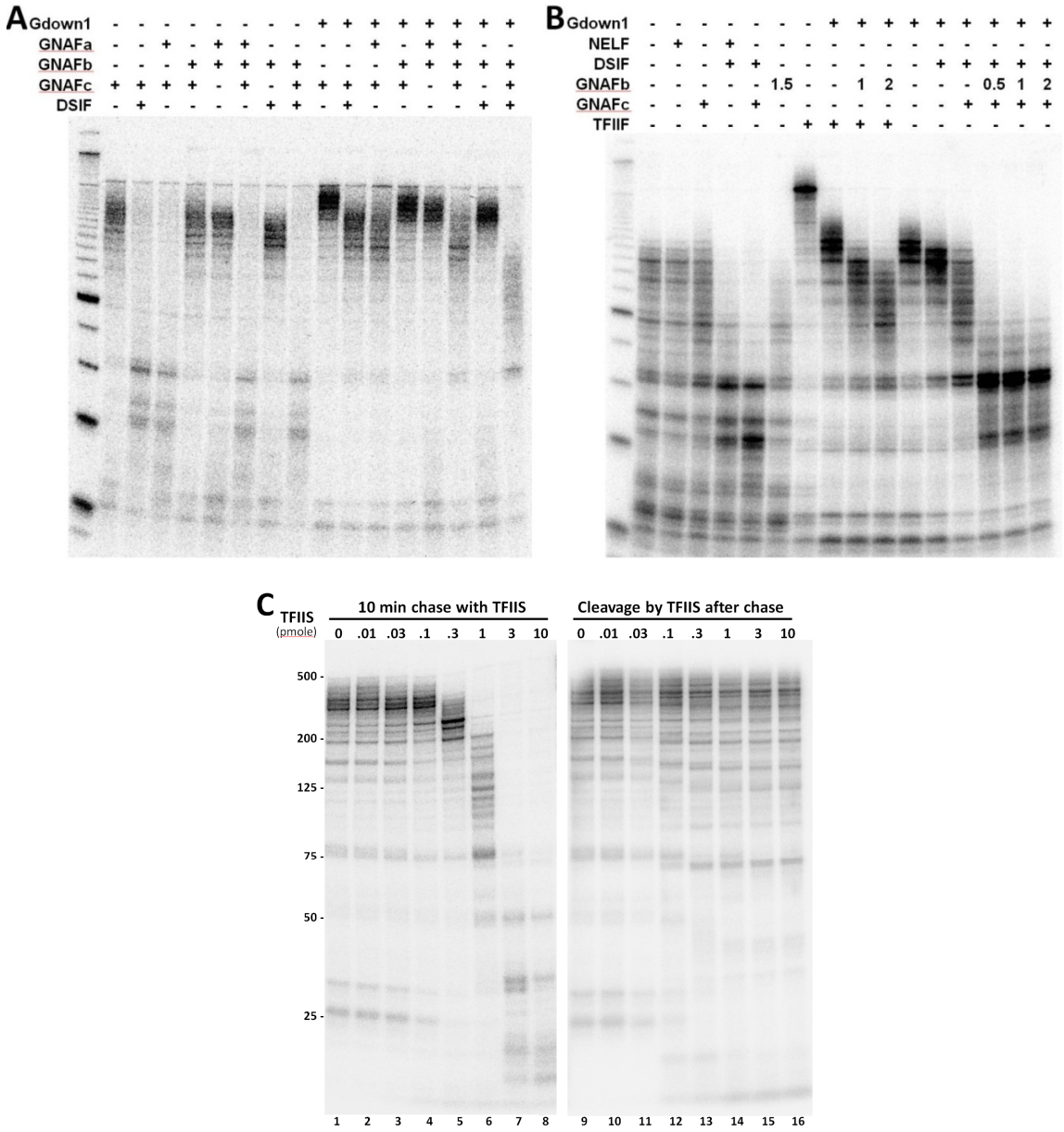

Figure S3. Identification of activities purified from HNE and demonstration of positive and negative effects of TFIIS.

Fractions from the purification scheme in Figure S2 were temporarily named GNAFa, GNAFb and GNAFc. The elongation assays in (**A**) and (**B**) have the indicated combinations of factors. DSIF substituted for GNAFa, NELF substituted for GNAFc, but no factor could be substituted for GNAFb which we now call GNAF. (**C**) Concentration dependent switch of TFIIS from a positive to negative elongation factor. The left panel shows a 10 minute chase of EECs in the presence of the indicated increasing amounts of TFIIS and the right panel shows a 10 minute incubation of the same concentrations of TFIIS and 3 mM $MgCl_2$ with elongation complexes that had been re-isolated after a 10 min. chase. The first evidence for suppression of pausing (lane 4) correlates with the appearance of transcript cleavage activity (lane 12). At higher concentrations TFIIS has an overall negative effect on elongation by causing transcript cleavage at pause sites.

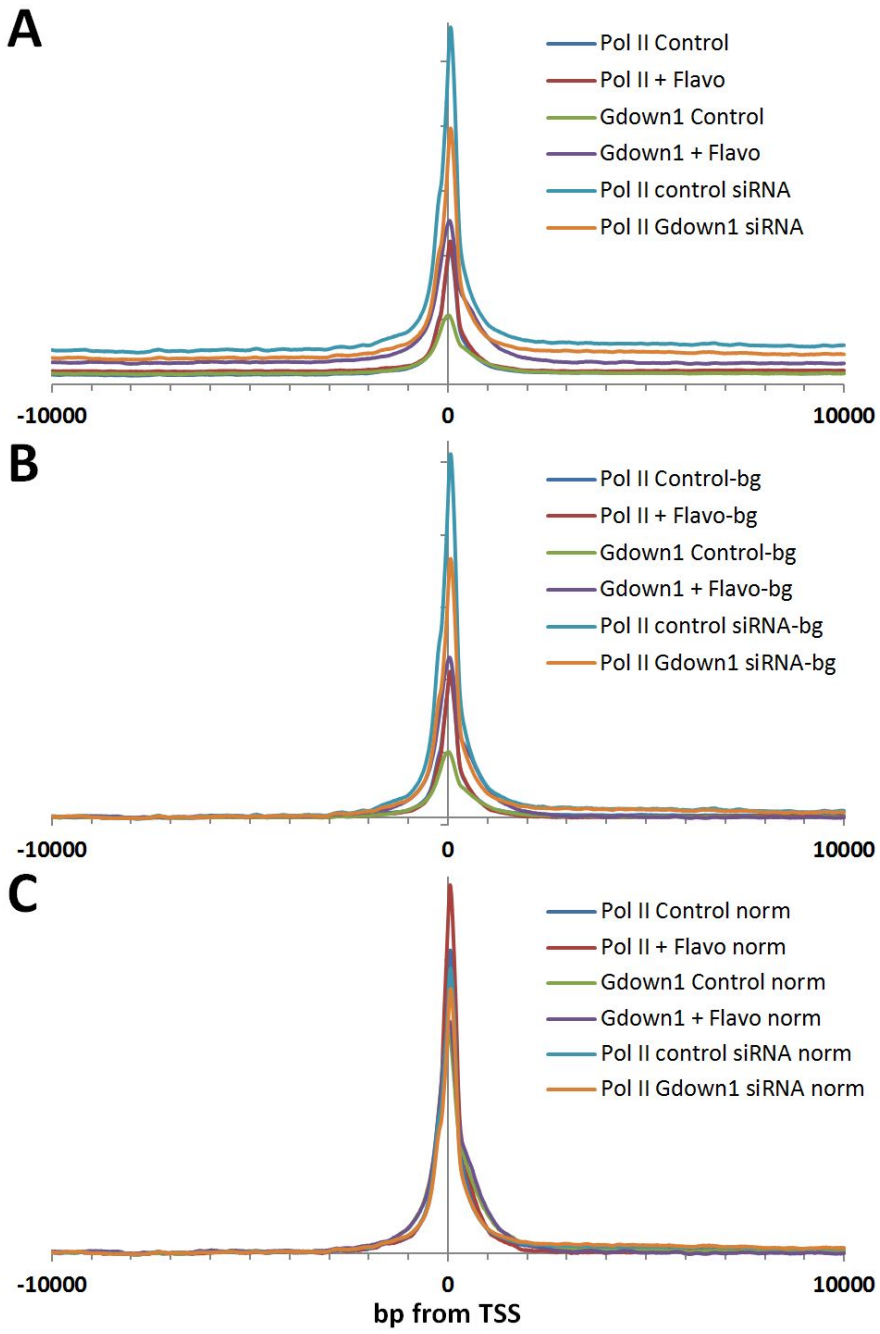

Figure S4. Background subtraction and normalization of ChIP-Seq data.
A custom set of annotated all RefSeq genes was produced by eliminating redundant entries for TSSs around a single gene and then eliminating all genes with a TSS within 1000 bp of another. All fragments from the indicated datasets uniquely aligned to hg18 reference genome were mapped within 10,000 bp of the TSSs, and the number of reads were summed at each position. The lowest 2000 values for individual base pairs (10% of data) were averaged and this was subtracted from each position. The resulting data was then normalized so that the area under each curve was equal. (**A**) Raw data; (**B**) Background subtracted data; (**C**) Normalized data. The final dataset accurately depicts the relative (not absolute) occupancy of the indicated protein across the region.

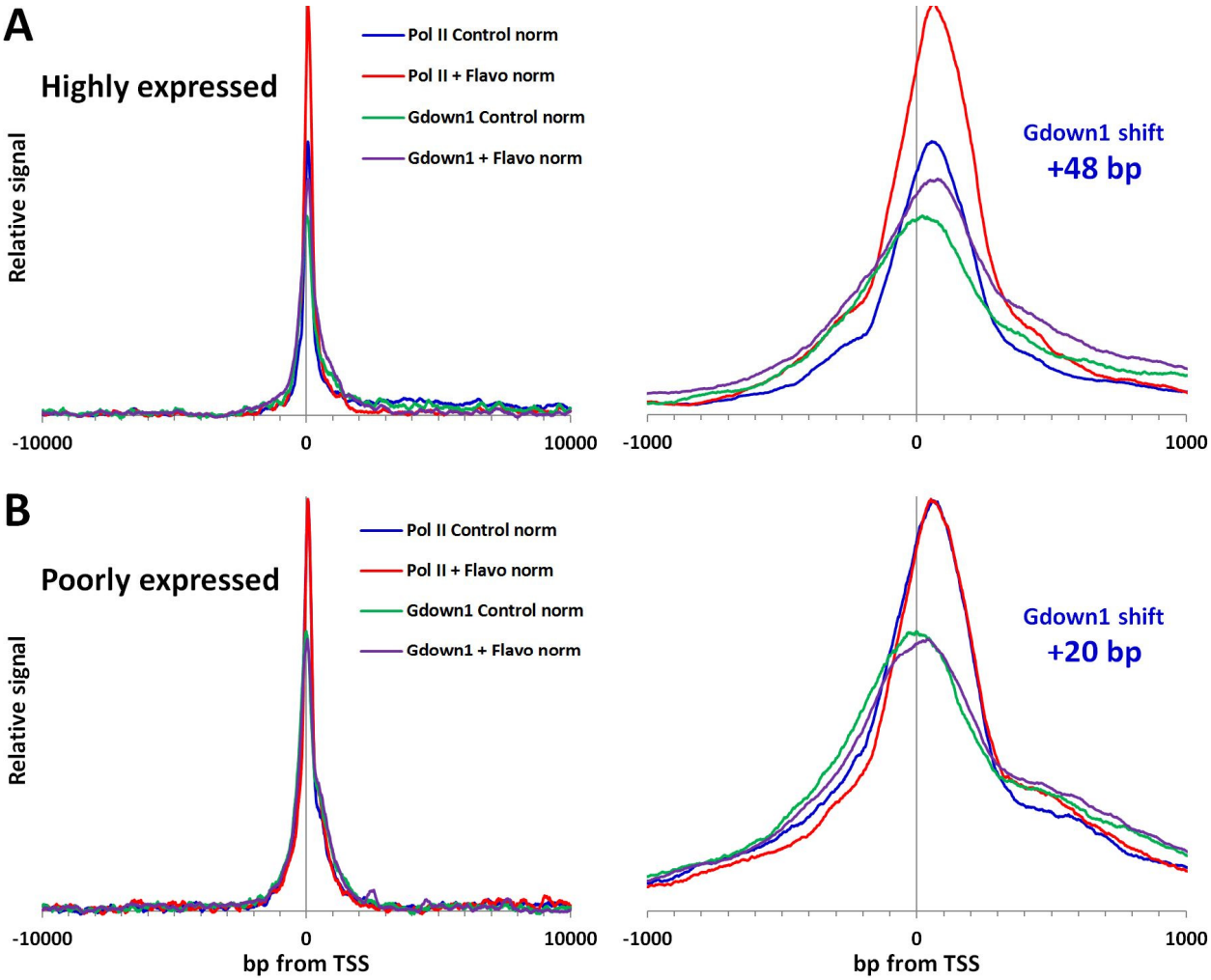

Figure S5. Average distribution of Pol II and Gdown1 for selected genes.
Pol II and Gdown1 ChIP-Seq data (+/- FP) were treated as in Figure S4 to subtract background and normalize to total area under the curves for the -10 kb to +10 kb region around the TSS for the indicated groups of genes (**A**) Highly expressed genes. Top 200 genes ranked by expression level in HeLa cells by RNA-Seq (http://www.ncbi.nlm.nih.gov/geo/query/acc.cgi?acc=GSE23316) from a list of genes that did not contain TSSs with 1000 bp of each other. (**B**) Poorly expressed genes. Genes ranked 4000 to 5000 by amount of Pol II in the -500 to +500 bp region around the TSS from a list of 13,899 genes that had no TSSs or transcription end sites within 1000 bp of each other. Note that the increase in poised Pol II after FP treatment due to loss of downstream Pol II and the normalization procedure was relatively large in **A** and very small in **B**. The shift in the peak of Gdown1 and Pol II were determined using the peak finding program used in Figure 7 and the shift of Gdown1 indicated. The Pol II shift was +17 bp and +21 bp for **A** and **B**, respectively.

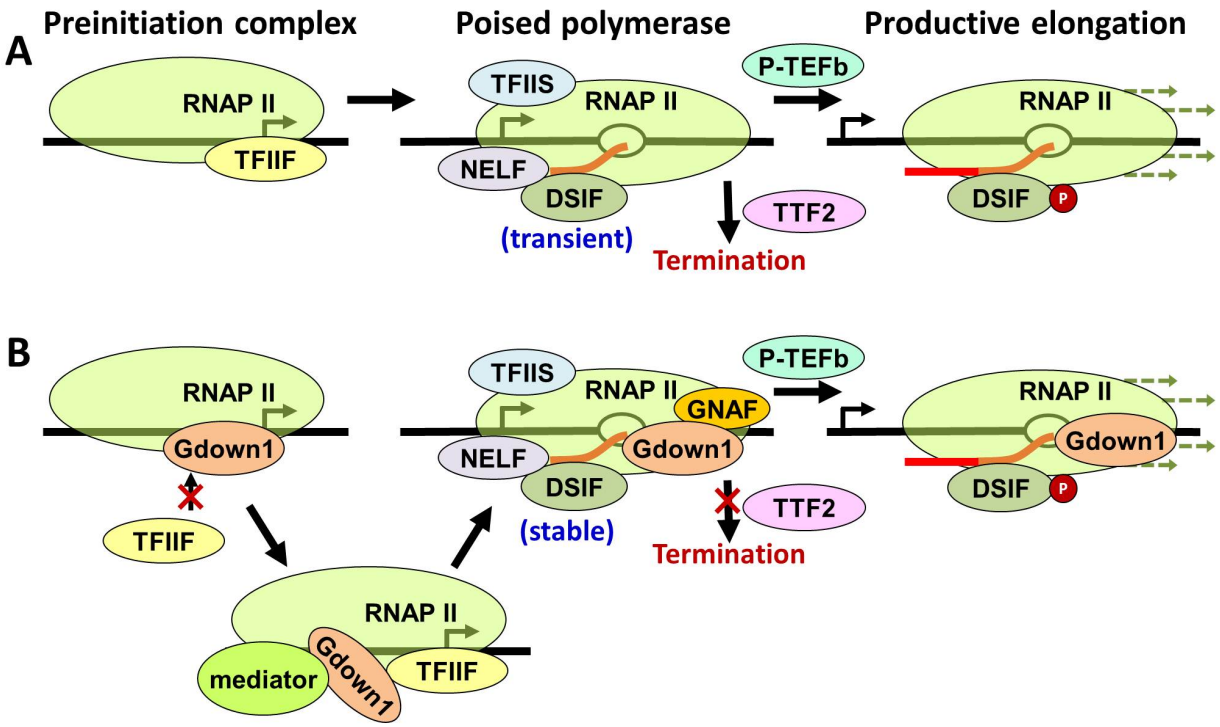

Figure S6. Model of Gdown1 function.
The diagram depicts initiation, promoter proximal pausing and productive elongation for polymerases with or without Gdown1. (**A**) Without Gdown1, Pol II forms a PIC with TFIIF and after initiation comes under the control of DSIF, NELF and TFIIS generating a transiently poised polymerase that can either enter productive elongation through the action of P-TEFb or terminate due to TTF2. (**B**) With Gdown1, an inactive PIC forms that requires mediator to remodel Gdown1 thereby allowing TFIIF to bind. Initiation with Pol II containing Gdown1 allows formation of a stably poised polymerase under the control of DSIF, NELF, TFIIS, and the Gdown1 Negative Accessory Factor, GNAF. These polymerases cannot be terminated by TTF2, but can enter productive elongation through the action of P-TEFb.

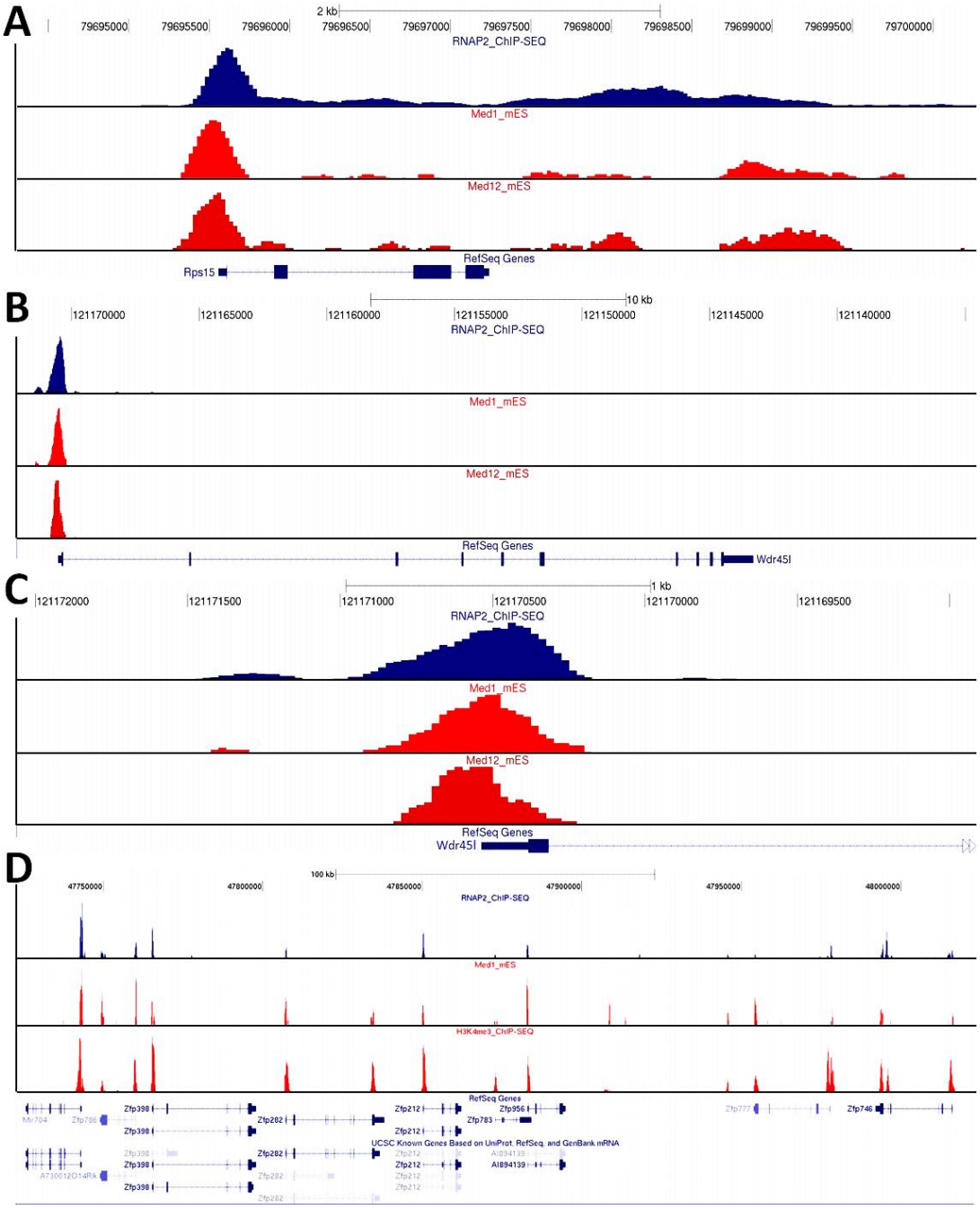

Figure. S7. Mediator ChIP-Seq in mouse embryonic stem cells.
Published ChIP-Seq data sets for the mediator subunits Med1 and Med12, as well as for H3K4me3 and Pol II from mouse embryonic stem cells (Kagey et al., 2010) were uploaded to the Genome Browser. (**A**) The highly expressed ribosomal subunit gene, *RPS15*, showing the entire transcribed region. The complete potentially transcribed region (**B**) and the promoter proximal region (**C**) of a poorly expressed gene, *WDR45L*. Note that in both of examples the peaks of mediator subunits are shifted upstream of the peak of poised polymerase. (**D**) Another region showing a variety of poorly expressed genes with only poised polymerases correlating with Med1.

Supplemental Experimental Procedures

Expression and purification of Gdown1 proteins

Human and bovine Gdown1 expression plasmids were constructed using pET151 vector (Invitrogen) and the bovine protein was purified as described previously (Hu et al., 2006). The recombinant His-tagged human Gdown1 protein was expressed in *Escherichia coli* BL21cells (Invitrogen) by overnight induction with 0.1 mM isopropyl 1-thio-β-D-galactopyranoside at 18^{o}C. Purification on Ni-NTA resin (Qiagen) was carried out as previously described (Byers et al., 2005). The protein was further purified by loading onto a 1-mL Mono Q column and elution with a linear gradient from 75-650 mM HGKEDP (25 mM HEPES, pH 7.6, 15% glycerol, 75-650 mM KCl, 0.1 mM EDTA, 1 mM DTT and 0.1 % of a saturated PMSF isopropanol solution). The resulting human Gdown1 protein was aliquotted and stored at -80^{o}C. SDS PAGE and silver staining for one of the final eluted fractions is shown in Figure S1.

Generation and affinity purification of human Gdown1 antibody

About 1.5 mg of recombinant His-tagged human Gdown1 protein was injected into a sheep to produce antibodies (Elmira Biologicals). This antiserum is available from Millipore. The affinity purification of antibody was performed using Actigel ADL resin (Sterogene) as previously described (Byers et al., 2005). A western blot of whole HeLa cell lysate probed with the affinity purified antibody is shown in Figure S1. The Gdown1 antiserum is available from Millipore.

Fractionation of HeLa nuclear extract

0.5 mL of HNE in 300 mM HGKE (25 mM HEPES, pH 7.6, 15% glycerol, 300 mM KCl, 0.1 mM EDTA) was diluted four fold with HGEDP (25 mM HEPES, pH 7.6, 15% glycerol, 0.1 mM EDTA, 1 mM DTT, and 0.1% PMSF) to lower the salt concentration to 75 mM. The diluted extract was incubated on ice for 10 minute, and then spun down at 17,000 g for 20 minutes at 4^{o}C. The supernatant was loaded onto a 1-mL Mono Q column that was pre-equilibrated with 75 mM HGKEDP and flow-through fractions were collected in fractions #1-5. Then the column was washed with 5 column volumes of 75 mM HGKEDP (collected in fractions #6-10) followed by elution with a linear gradient from 75 to 500 mM HGKEDP (fraction #11-20). Then the salt concentration was raised to 1 M and the rest of the column bound material was eluted, collected and concentrated as fraction #21. All fractions were stored at -80^{o}C.

***In vitro* transcription assays**

Immobilized templates used, the generation and isolation of early elongation complexes and in vitro transcription assays were as described earlier (Cheng and Price, 2007, 2009). Basically, elongation complexes containing RNA mostly less than 25 nt in length were generated by initiation on immobilized templates under pulse labeling conditions (30 seconds at 500 μM A,U, and GTP and 1 μM ^{32}P-CTP). The elongation complexes were washed with 1.6 M salt to remove all factors and then chased (500 μM of all NTPs) in the presence of the indicated factors for indicated periods of time. Except where indicated bovine Gdown1 was used in add back assays with the factor because the human and bovine factor had identical activity. The resulting labeled transcripts were analyzed in denaturing RNA gels and after drying the gels were subjected to autoradiography or phosphorimaging. Since the label is incorporated into first 25 nt of the transcripts, as the transcripts are extended they do not get hotter. Therefore, the pattern of transcripts seen is a faithful readout of the elongation properties of the polymerases (Cheng and Price, 2009).

Termination assays were carried out in the absence or presence of active transcription. To analyze termination of stalled elongation complexes, isolated elongation complexes were incubated with the

indicated amount of TTF2 for 5 minutes at room temperature in the presence of only 500 μM ATP. To terminate the transcribing elongation complexes, isolated elongation complexes were supplemented with TTF2 (and other protein(s) in some reactions as indicated) and then elongation was carried out for 5 minutes upon the addition of NTPs to 500 μM. In both cases, the termination reactions were stopped by adding EDTA to 20 mM. Then the reaction tubes were put into a magnetic particle concentrator (Invitrogen) for separation of the supernatant fraction from the paramagnetic beads. Transcripts in both fractions were extracted respectively and analyzed on a denaturing RNA gel.

Elongation complex electrophoretic mobility shift assays were carried out using the protocol described previously (Cheng and Price, 2008).

Chromatin immunoprecipitation (ChIP) and sequencing

ChIP assays were performed using the protocol described by Lee et al. (Lee et al., 2006). HeLa cells were maintained at 5% CO_2 and 37°C in DMEM plus 10% FBS (Hyclone). Cells were grown in T-150 flasks to 90% confluence and treated for one hour with FP (final concentration 1 μM with 0.1% DMSO) or 0.1% DMSO alone. For each immunoprecipitation, 5 x 10^7-1 x 10^8 cells were used. 1/10 volume of fresh 11% paraformaldehyde solution [11% paraformaldehyde (EM Grade, EMS), 50 mM HEPES-KOH, pH 7.5, 100 mM NaCl, and 1 mM EDTA] was added directly into the plates and cells were cross-linked for 15 minutes at room temperature. Cross-linking was stopped by addition of glycine to 125 mM final concentration. Cells were washed twice with cold PBS and harvested using a silicon scraper. Cells for each immunoprecipitation were pelleted in PBS and resuspended in 10 mL of ice cold Lysis Buffer 1 (50 mM HEPES-KOH, pH 7.5, 140 mM NaCl, 1 mM EDTA, 10% glycerol, 0.5% NP-40, and 0.25% Triton X-100). Cells were incubated at 4°C on a rocker for 10 minutes and then pelleted and resuspended in 10 mL of ice cold Lysis buffer 2 (10 mM Tris-HCl, pH 8.0, 100 mM NaCl and 1 mM EDTA). After 10 minute-incubation at 4°C on a rocker, the cells were pelleted and resuspended in 3.5 mL of ice cold Lysis buffer 3 (10 mM Tris-HCl, pH 8.0, 100 mM NaCl, 1 mM EDTA, 0.1% Sodium Deoxycholate, and 0.5% Sarkosyl). Samples were sonicated on ice using a Fisher Model 550 Sonic Dismembrator (Fisher Scientific) at a setting of 4 for eighteen 20-second pulses with 1 minute rests between pulses to generate DNA fragments <500 bp. After sonication, 1/10 volume of 10% Triton X-100 was added to the sonicated lysate and then the samples were spun at 20,000 g for 10 minutes at 4°C to pellet debris. 50 μL of the supernatant in each sample were saved as input DNA and the rest of the lysate was used for immunoprecipitation.

For each immunoprecipitation 100 μL of Protein G Dynabeads (Invitrogen) were used. The beads were washed with Block Solution (0.5% BSA in 1X PBS) three times and resuspended in 250 μL Block Solution. The beads were incubated with 10 μg of Pol II antibody at 4°C overnight. For ChIP-Seq, the N-20 antibody (Santa Cruz, sc-899) was used which recognizes the N-terminus of Rpb1. Then the beads were washed with Block Solution three times, resuspended in 100 μL of Block Solution, and incubated with the sonicated cell lysate at 4°C overnight. After the incubation, beads were washed four times with RIPA buffer (50 mM HEPES-KOH, pH7.5, 100 mM NaCl, 1 mM EDTA, 500 mM LiCl, 1% [v/v] NP-40, 0.7% Sodium Deoxycholate), once with a buffer containing TE and 50 mM NaCl. Immunocomplexes were eluted for 30 minutes at 65°C with Elution buffer (1% SDS, 50 mM Tris-HCl, pH 8.0, 10 mM EDTA) and the beads were removed with a magnetic concentrator. Reverse crosslinking was performed for both the immunoprecipitated DNA and for the input DNA samples (with 150 μL of Elution buffer added) by an incubation at 65°C for a minimum of six hours. DNA was purified through ethanol precipitation and then used for ChIP-Seq. The DNA fragments were isolated from an agarose gel, blunt-ended, ligated to the Solexa adaptors, and sequenced using the Illumina 1G Genome Analyzer as described previously (Barski et al., 2007; Rahl et al., 2010).

Data analysis

Raw sequences generated from Illumina/Solexa sequencer were aligned using ELAND software to NCBI Build 36.1 (UCSC hg18) of the human genome. Only sequences that mapped uniquely to the genome with zero or one mismatch were used for further analysis. When multiple sequences mapped to the same genomic position, a maximum of two reads mapping to the same position were used. The sequenced reads represent only the ends of each immunoprecipitated fragments instead of the precise protein-DNA binding sites. To illustrate the entire DNA fragment, the 3' end of each read was extended 200 bp. The reference genome was partitioned into 25 bp bins and the total reads (including partial reads) in each bin were summed and used to generate the visualization file in wiggle (WIG) format.

For Figures 5E, 6 and 7, the complete set of RefSeq genes was downloaded from the UCSC table browser on December 1, 2010. A custom annotated RefSeq gene list was generated by merging the all TSSs for each gene that were within 500 bases of each other. Then TSSs within 1000 bp of each other (6% of the total number) were removed from the list. This list was used for analyses in Figures 5D, 6, 7C-D, S4, and S6. A genomic coordinate file was compiled by extending the 3' end of each original sequence to a total of 200 bp. The number of reads within 10,000 bases of the TSS of each gene in the custom gene list was tabulated. Similar analysis was applied to the location of center of peaks generated from the peak finding algorithm for the region within 500 bp relative to the TSS. Heat maps were generated using the program R (www.r-project.org). Genes were rank ordered based on the sequence density for Pol II from -2K to +2K from the TSS. Using this order, basepair resolution sequence density for Pol II and Gdown1 for the top 20,000 genes was displayed without binning. The raw images were 20,000 x 4000 pixels each and both were adjusted identically using the gamma adjustment in Corel Photopaint to allow visualization of the wide range of data.

A peak finding algorithm (ChIP-Seq Peak) was designed to examine the data within individual WIG files and determine precise position and height of each significant peak. This algorithm assumes that each 200 bp immunoprecipitated DNA fragment is sequenced randomly from either end and that typical peaks would be approximately 400 bases wide at the base. Peaks less than 250 bp wide were eliminated and the center of each remaining peak was determined using Gaussian curve fitting. The height was determined by the area under each peak.

Supplemental References

Barski, A., Cuddapah, S., Cui, K., Roh, T.Y., Schones, D.E., Wang, Z., Wei, G., Chepelev, I., and Zhao, K. (2007). High-resolution profiling of histone methylations in the human genome. Cell *129*, 823-837.
Byers, S.A., Price, J.P., Cooper, J.J., Li, Q., and Price, D.H. (2005). HEXIM2, a HEXIM1-related protein, regulates positive transcription elongation factor b through association with 7SK. J Biol Chem *280*, 16360-16367.
Cheng, B., and Price, D.H. (2007). Properties of RNA polymerase II elongation complexes before and after the P-TEFb-mediated transition into productive elongation. J Biol Chem *282*, 21901-21912.
Cheng, B., and Price, D.H. (2008). Analysis of factor interactions with RNA polymerase II elongation complexes using a new electrophoretic mobility shift assay. Nucleic Acids Res *36*, e135.
Cheng, B., and Price, D.H. (2009). Isolation and functional analysis of RNA polymerase II elongation complexes. Methods *48*, 346-352.
Hu, X., Malik, S., Negroiu, C.C., Hubbard, K., Velalar, C.N., Hampton, B., Grosu, D., Catalano, J., Roeder, R.G., and Gnatt, A. (2006). A Mediator-responsive form of metazoan RNA polymerase II. Proc Natl Acad Sci U S A *103*, 9506-9511.
Kagey, M.H., Newman, J.J., Bilodeau, S., Zhan, Y., Orlando, D.A., van Berkum, N.L., Ebmeier, C.C., Goossens, J., Rahl, P.B., Levine, S.S*., et al.* (2010). Mediator and cohesin connect gene expression and chromatin architecture. Nature *467*, 430-435.
Lee, T.I., Johnstone, S.E., and Young, R.A. (2006). Chromatin immunoprecipitation and microarray-based analysis of protein location. Nature protocols *1*, 729-748.
Rahl, P.B., Lin, C.Y., Seila, A.C., Flynn, R.A., McCuine, S., Burge, C.B., Sharp, P.A., and Young, R.A. (2010). c-Myc regulates transcriptional pause release. Cell *141*, 432-445.

ER Tubules Mark Sites of Mitochondrial Division

Jonathan R. Friedman *et al.*

Science **334**, 358 (2011);
DOI: 10.1126/science.1207385

Science (print ISSN 0036-8075; online ISSN 1095-9203) is published weekly, except the last week in December, by the American Association for the Advancement of Science, 1200 New York Avenue NW, Washington, DC 20005.

in a single cell, noise can substantially restrict the amount of information transduced about input intensity, particularly within individual signaling pathways. The bush and tree network models, which provide a unified theoretical framework for analyzing branched motifs widespread in natural and synthetic signaling networks, further demonstrated that signaling networks can be more effective in information transfer, although bottlenecks can also severely limit the information gained. Receptor-level bottlenecks restrict the TNF and also PDGF signaling networks (fig. S11) and may be prevalent in other signaling systems.

We explored several strategies that a cell might use to overcome restrictions due to noise. We found that negative feedback can suppress bottleneck noise, which can be offset by concomitantly reduced dynamic range of the response. Time integration can increase the information transferred, to the extent that the response undergoes substantial dynamic fluctuations in a single cell over the physiologically relevant time course. The advantage of collective cell responses can also be substantial, but limited by the number of cells exposed to the same signal or by the information present in the initiating signal itself.

Responses incorporating the signaling history of the cell might also increase the information (*40*, *41*). For instance, responses relative to the basal state (fold-change response) might be less susceptible to noise arising from diverse initial states (*23*), although this does not necessarily translate into large amounts of transferred information (table S1). Similarly, for the reporter gene system described here (fig. S12), ~0.5 bits of additional information can be obtained if a cell can determine expression levels at both early and late time points. However, noise in the biochemical networks that a cell uses to record earlier output levels and to later compute the final response may nullify the information gain potentially provided by this strategy. Overall, we anticipate that the information theory paradigm can extend to the analysis of noise-mitigation strategies and information-transfer mechanisms beyond those explored here, in order to determine what specific signaling systems can do reliably despite noise.

References and Notes

1. J. G. Albeck, J. M. Burke, S. L. Spencer, D. A. Lauffenburger, P. K. Sorger, *PLoS Biol.* **6**, e299 (2008).
2. N. Rosenfeld, J. W. Young, U. Alon, P. S. Swain, M. B. Elowitz, *Science* **307**, 1962 (2005).
3. T. J. Perkins, P. S. Swain, *Mol. Syst. Biol.* **5**, 326 (2009).
4. W. J. Blake, M. Kaern, C. R. Cantor, J. J. Collins, *Nature* **422**, 633 (2003).
5. M. B. Elowitz, A. J. Levine, E. D. Siggia, P. S. Swain, *Science* **297**, 1183 (2002).
6. J. Paulsson, *Nature* **427**, 415 (2004).
7. J. M. Pedraza, A. van Oudenaarden, *Science* **307**, 1965 (2005).
8. J. M. Raser, E. K. O'Shea, *Science* **304**, 1811 (2004).
9. T. M. Cover, J. A. Thomas, *Elements of Information Theory* (Wiley, New York, 1991).
10. R. R. de Ruyter van Steveninck, G. D. Lewen, S. P. Strong, R. Koberle, W. Bialek, *Science* **275**, 1805 (1997).
11. D. Fuller *et al.*, *Proc. Natl. Acad. Sci. U.S.A.* **107**, 9656 (2010).
12. E. Ziv, I. Nemenman, C. H. Wiggins, *PLoS ONE* **2**, e1077 (2007).
13. G. Tkacik, C. G. Callan Jr., W. Bialek, *Proc. Natl. Acad. Sci. U.S.A.* **105**, 12265 (2008).
14. P. Mehta, S. Goyal, T. Long, B. L. Bassler, N. S. Wingreen, *Mol. Syst. Biol.* **5**, 325 (2009).
15. R. Cheong, A. Hoffmann, A. Levchenko, *Mol. Syst. Biol.* **4**, 192 (2008).
16. R. Cheong, C. J. Wang, A. Levchenko, *Mol. Cell. Proteomics* **8**, 433 (2009).
17. S. L. Werner *et al.*, *Genes Dev.* **22**, 2093 (2008).
18. S. Tay *et al.*, *Nature* **466**, 267 (2010).
19. L. Ashall *et al.*, *Science* **324**, 242 (2009).
20. D. E. Nelson *et al.*, *Science* **306**, 704 (2004).
21. R. Cheong *et al.*, *J. Biol. Chem.* **281**, 2945 (2006).
22. A. Hoffmann, A. Levchenko, M. L. Scott, D. Baltimore, *Science* **298**, 1241 (2002).
23. C. Cohen-Saidon, A. A. Cohen, A. Sigal, Y. Liron, U. Alon, *Mol. Cell* **36**, 885 (2009).
24. X. R. Bao, I. D. Fraser, E. A. Wall, S. R. Quake, M. I. Simon, *Biophys. J.* **99**, 2414 (2010).
25. M. Coppey, A. N. Boettiger, A. M. Berezhkovskii, S. Y. Shvartsman, *Curr. Biol.* **18**, 915 (2008).
26. B. B. Averbeck, P. E. Latham, A. Pouget, *Nat. Rev. Neurosci.* **7**, 358 (2006).
27. J. W. Pillow *et al.*, *Nature* **454**, 995 (2008).
28. E. Schneidman, W. Bialek, M. J. Berry II, *J. Neurosci.* **23**, 11539 (2003).
29. H. Wajant, K. Pfizenmaier, P. Scheurich, *Cell Death Differ.* **10**, 45 (2003).
30. A. Becskei, L. Serrano, *Nature* **405**, 590 (2000).
31. I. Lestas, G. Vinnicombe, J. Paulsson, *Nature* **467**, 174 (2010).
32. R. C. Yu *et al.*, *Nature* **456**, 755 (2008).
33. I. E. Wertz *et al.*, *Nature* **430**, 694 (2004).
34. E. G. Lee *et al.*, *Science* **289**, 2350 (2000).
35. V. Shahrezaei, P. S. Swain, *Proc. Natl. Acad. Sci. U.S.A.* **105**, 17256 (2008).
36. S. Krishna, M. H. Jensen, K. Sneppen, *Proc. Natl. Acad. Sci. U.S.A.* **103**, 10840 (2006).
37. S. Thierfelder, K. Ostermann, A. Göbel, G. Rödel, *Appl. Biochem. Biotechnol.* **163**, 954 (2011).
38. K. Francis, B. O. Palsson, *Proc. Natl. Acad. Sci. U.S.A.* **94**, 12258 (1997).
39. J. Parkin, B. Cohen, *Lancet* **357**, 1777 (2001).
40. I. Nemenman, G. D. Lewen, W. Bialek, R. R. de Ruyter van Steveninck, *PLOS Comput. Biol.* **4**, e1000025 (2008).
41. S. P. Strong, R. Koberle, R. R. de Ruyter van Steveninck, W. Bialek, *Phys. Rev. Lett.* **80**, 197 (1998).

Acknowledgments: We thank A. Hoffmann, M. Simon, S. Shvartsman, C. Cohen-Saidon, and U. Alon for sharing data and materials; A. Ganesan and H. Chang for experimental assistance; and P. Iglesias, Y. Qi, and A. Feinberg for insightful discussions and reviewing drafts of the manuscript. This work was supported by NIH grants GM072024 and RR020839 (R.C., A.R., C.J.W., and A.L.) and CA132629 (I.N.), the Medical Scientist Training Program at the Johns Hopkins University (R.C.), and, in early stages of the work, the Los Alamos National Laboratory Directed Research and Development program (I.N.).

Supporting Online Material

www.sciencemag.org/cgi/content/full/science.1204553/DC1
Materials and Methods
SOM Text
Figs. S1 to S12
Table S1
References (*42*–*55*)

18 February 2011; accepted 7 September 2011
Published online 15 September 2011;
10.1126/science.1204553

ER Tubules Mark Sites of Mitochondrial Division

Jonathan R. Friedman,[1] Laura L. Lackner,[2] Matthew West,[1] Jared R. DiBenedetto,[1] Jodi Nunnari,[2] Gia K. Voeltz[1]*

Mitochondrial structure and distribution are regulated by division and fusion events. Mitochondrial division is regulated by Dnm1/Drp1, a dynamin-related protein that forms helices around mitochondria to mediate fission. Little is known about what determines sites of mitochondrial fission within the mitochondrial network. The endoplasmic reticulum (ER) and mitochondria exhibit tightly coupled dynamics and have extensive contacts. We tested whether ER plays a role in mitochondrial division. We found that mitochondrial division occurred at positions where ER tubules contacted mitochondria and mediated constriction before Drp1 recruitment. Thus, ER tubules may play an active role in defining the position of mitochondrial division sites.

Regulation of mitochondrial division is critical to normal cellular function; excess division is linked to numerous diseases, including neurodegeneration and diabetes (*1*, *2*). The central player in mitochondrial division is the highly conserved dynamin-related protein (Drp1 in mammals, Dnm1 in yeast), which belongs to a family of large guanosine triphosphatases (GTPases) that self-assemble to regulate membrane structure (*3*). Division dynamins are likely to work by oligomerizing in a GTP-dependent manner into helices that wrap around mitochondria; locally controlled assembly-stimulated GTP hydrolysis is thought to provide the mechanochemical force that completes fission of the outer and inner membranes (*4*). There are additional proteins required for mitochondrial division, such as the outer membrane protein Mff (mitochondrial fission factor), which is present only in mammals (*5*). Although general mechanisms exist for

[1]Department of Molecular, Cellular, and Developmental Biology, University of Colorado, Boulder, CO 80309, USA. [2]Department of Molecular and Cellular Biology, University of California, Davis, CA 95616, USA.

*To whom correspondence should be addressed. E-mail: gia.voeltz@colorado.edu

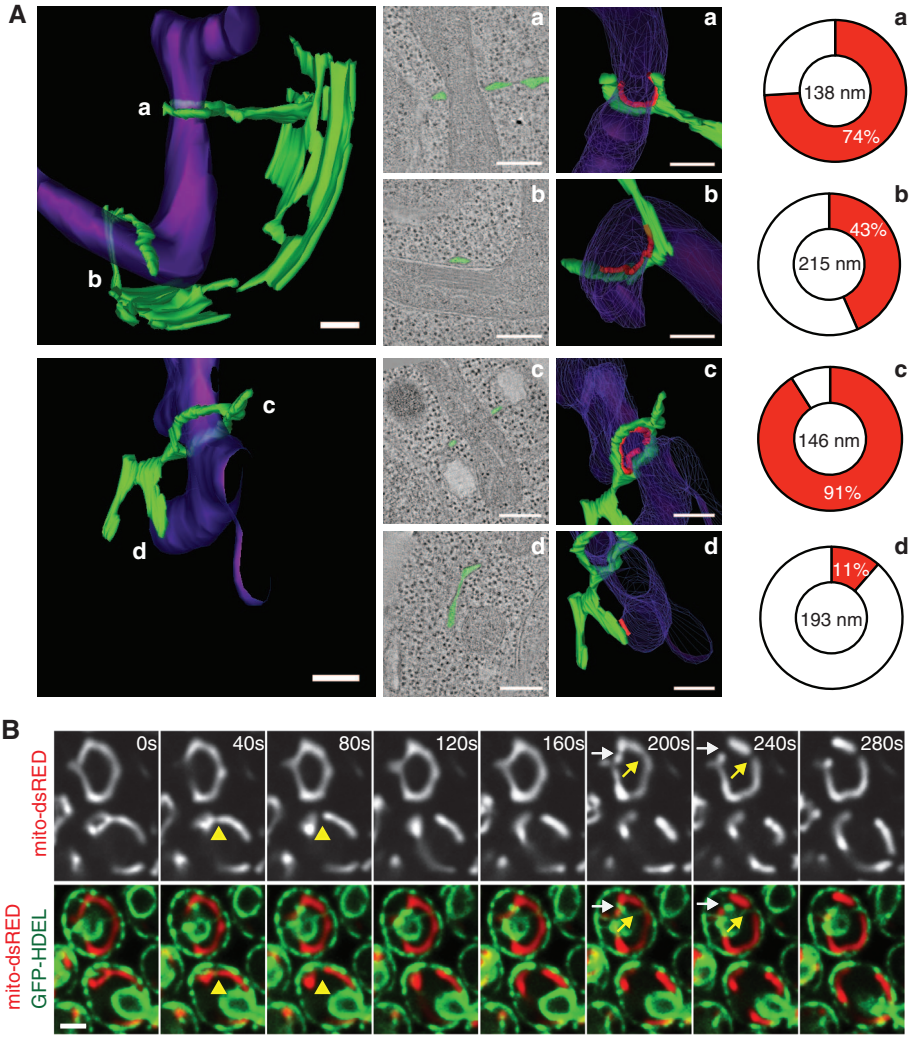

Fig. 1. Mitochondrial constriction and division occurs at ER-mitochondrial contacts in yeast. (**A**) The 3D models (left images) of ER (green) and mitochondria (purple) at contact domains were imaged by EM and tomography of high-pressure frozen yeast cells. Middle images are 2D tomographs of contact sites (second column, ER drawn in green) and the corresponding 3D models of each (third column). Contact, marked in red, is defined as regions where the ER membrane comes within 30 nm of the mitochondrial membrane, and ribosomes are excluded (third column). Right schematics demonstrate the percentage of the mitochondrial circumference that makes contact with the ER membrane [red is contact, white is not (*19*)]. The diameter of each mitochondrion at positions of ER contact is shown. Regions where the mitochondria are constricted (models a and c) have a high percent of ER wrapping. Additional EM tomographs and analysis of constrictions are shown in fig. S1, A and B. (**B**) Time-lapse images of yeast cells expressing mito-dsRed and GFP-HDEL (ER). A single focal plane is shown. Arrows and arrowheads indicate sites of mitochondrial division. A corresponding z-series is shown in fig. S1C. Scale bars indicate, in (A), 200 nm; (B), 2 μm.

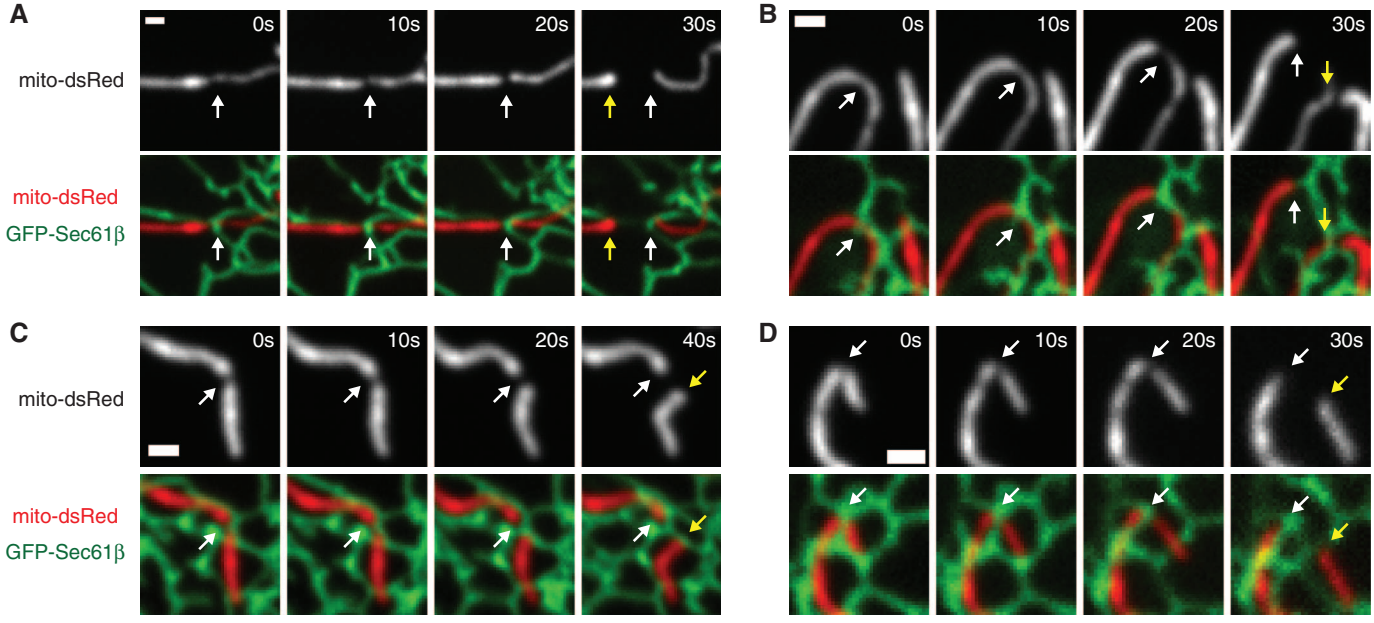

Fig. 2. Mitochondrial division occurs at ER-mitochondrial contact sites in mammalian cells. (**A** to **D**) Four examples of mitochondrial division over time courses shown in Cos-7 cells expressing GFP-Sec61β (ER) and mito-dsRed. The site of mitochondrial division (white arrows) and the position of the newly formed mitochondrial ends (yellow arrows) are shown. Additional examples are included in fig. S2A. Scale bars, 1 μm.

recruiting Dnm1 or Drp1 to mitochondria, it is not known whether there are specific sites on mitochondria that are marked for division (*6*). Furthermore, both Dnm1 and Drp1 oligomerize into helices that are much smaller than the diameter of mitochondria (Dnm1 helices have reported mean diameters of 109 nm in yeast and 129 nm in vitro), suggesting that Dnm1 (Drp1)–independent mitochondrial constriction may be needed to facilitate mitochondrial division (*4*, *6*–*9*).

Contact sites exist between mitochondria and the endoplasmic reticulum (ER) and are important for phospholipid synthesis and calcium signaling [for review, see (*10*)]. Based on recent data, there are likely several types of molecular bridges that mediate these contacts, such as the ERMES complex identified in yeast and the mitochondrial fusion protein mitofusin 2 (Mfn2) in mammalian cells (*11*, *12*). These physical contacts are persistent and maintained under dynamic conditions (*13*), suggesting that the ER-mitochondrial interface is vital for function. We have used electron microscopy (EM) and tomography to analyze the three-dimensional (3D) structure of contacts between the ER and mitochondria in the yeast *Saccharomyces cerevisiae*. We observed the high-resolution (~4 nm) structure and 3D models of four ER-mitochondrial contacts taken from two cells (Fig. 1A). In these examples, the ER was wrapped around mitochondria to varying degrees. In two of the four examples, the ER almost completely circumscribed the mitochondrial outer membrane, and mitochondria were constricted at the point of contact (mitochondrial diameter 138 nm and 146 nm circumscribed versus 215 nm and 193 nm uncircumscribed at ER contact) (Fig. 1A; fig. S1, A and B; and movies S1 and S2). These data suggest that ER tubules associate with and may mediate mitochondrial constriction sites.

We thus examined the role of ER in mitochondrial division by using fluorescence microscopy in live yeast cells transformed with an ER marker (GFP-HDEL) and mito-dsRed to image the behavior of ER and mitochondria simultaneously over time. The vast majority of mitochondrial division events were spatially linked to sites of ER-mitochondrial contact (87%, $n = 112$

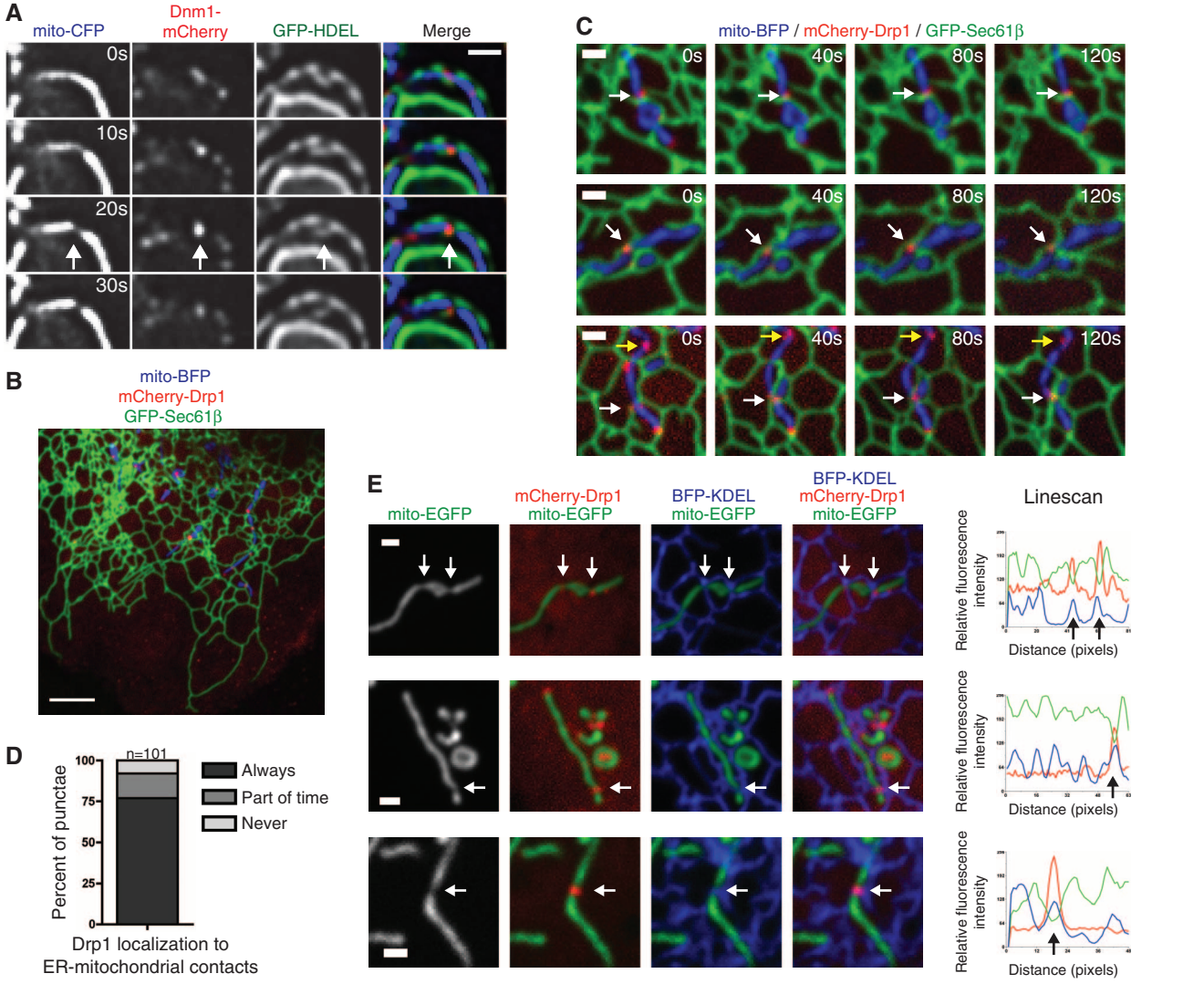

Fig. 3. Dnm1- and Drp1-mediated mitochondrial division occurs at ER contact sites. (**A**) Time-lapse images of wild-type yeast cells expressing mito-CFP, GFP-HDEL (ER), and Dnm1-mCherry. A single focal plane is shown. Arrows indicate the site of mitochondrial division, which is marked by both ER-mitochondria contact and Dnm1. (**B**) Merged image of a live Cos-7 cell expressing GFP-Sec61β (ER), mito-BFP, and mCherry-Drp1. (**C**) Examples of cells as in (B) that show that Drp1 punctae maintain colocalization with positions of ER-mitochondrial contact over time. White arrows indicate Drp1 punctae that maintain contact with both the ER and mitochondria. Yellow arrows indicate a rare example of Drp1 that does not contact the ER. (**D**) The percentage of mitochondrial Drp1 punctae that colocalize with the ER membrane over a 2-min time course. (**E**) Examples of mitochondrial constrictions at ER contact sites marked by Drp1. Left-hand images show Cos-7 cells expressing mito-EGFP, BFP-KDEL (ER), and mCherry-Drp1, merged as indicated. Right graphs are line scans drawn through the mitochondria and show the relative fluorescence intensity of mitochondria (green), ER (blue), and Drp1 (red) along its length. White arrows at constrictions on images correspond to black arrows shown on the line scan. Additional examples are shown in fig. S4. Scale bars for (A), (C), and (E), 1 μm; (B), 5 μm.

from 281 cells) (Fig. 1B). ER tubules crossed over (Fig. 1B, yellow arrows) and wrapped around mitochondria (Fig. 1B, white arrows, and fig. S1C). At ER-mitochondrial contact sites, mitochondrial constriction followed by mitochondrial division was observed (Fig. 1B).

We next tested whether ER plays a similar role in mammalian mitochondrial division by using fluorescence microscopy of live Cos-7 cells transiently transfected with fluorescent markers for ER (GFP-Sec61β) and mitochondria (mito-dsRed). We imaged regions of the cell periphery where contacts between the mitochondria and ER were well resolved and observed that mitochondrial division events predominantly occurred at sites of contact between ER and mitochondria (94%, $n = 32$ from 23 cells) (Fig. 2, fig. S2A, and movies S3 and S4). Furthermore, the majority of events (88%) were sites of ER tubules crossing over the mitochondria, suggesting that the structural context of the interaction is important. The frequency of ER-associated mitochondrial division is much higher than would be predicted on the basis of the area of mitochondria covered by crossing ER tubules as determined by colocalization of mitochondrial and ER markers (fig. S2B).

Thus, in both yeast and mammalian cells, ER tubules are at mitochondrial division sites and may be involved in mitochondrial constriction during this process. Next, we asked whether mitochondrial division occurs in yeast cells that have substantially reduced levels of tubules because of the absence of the membrane shaping proteins Rtns and Yop1 (*14*, *15*). By using both EM and fluorescence microscopic analyses, we observed that, in regions of mutant cells in which ER tubules were dramatically reduced, short ER tubules extended out of the massive ER cisternae and associated with mitochondrial constrictions and division events (fig. S3). Thus, ER tubules are a consistent feature of ER contact at mitochondrial constrictions, even under conditions where most tubules are depleted. Furthermore, Rtns and Yop1 are dispensable for the biogenesis of the ER tubules that associate with mitochondrial division events.

To ask whether ER-associated division events are spatially linked to the mitochondrial division machinery, we determined the relationship of ER-mitochondrial contacts to the division dynamins Dnm1 and Drp1. Dnm1 and Drp1 assemble into punctate structures at steady state, and a subset of these structures are found on mitochondria and at mitochondrial division sites (*6*, *16*, *17*). We imaged live yeast transformed with Dnm1-mCherry, mito–cyan fluorescent protein (CFP), and GFP-HDEL (ER) and observed that a large percentage of Dnm1 punctae were at sites of mitochondrial-ER contact (46%, $n = 225$). These Dnm1 punctae could be observed at sites where ER tubule crossover and mitochondrial division occurred (Fig. 3A). In Cos-7 cells transiently transfected with GFP-Sec61β (ER), mito–blue fluorescent protein (BFP), and mCherry-Drp1, we observed that the majority of Drp1 punctae stably associated with mitochondria and localized to ER-mitochondrial contacts over time (Fig. 3, B to D, and movie S5). Furthermore, a subset of Drp1 at these contacts was associated with a mitochondrial constriction site (78%, excluding punctae localized to mitochondrial tips, $n = 50$). The mitochondrial constrictions marked by Drp1 punctae were always either at ER tubule crossovers (81%) or adjacent to them (19%) (Fig. 3E and fig. S4). Together, the localization of the mitochondrial division dynamins in yeast and mammalian cells to regions of ER-mitochondrial contacts and the observations that these regions are associated with constricted mitochondria and subsequent division indicate a direct role of the ER in the process of mitochondrial division.

Mff is a mammalian-specific mitochondrial outer membrane protein required for mitochondrial localization of Drp1 and division (*5*, *18*). Drp1 and Mff colocalize in punctate structures on mitochondria, and Mff punctae persist in cells where Drp1 expression is reduced by RNAi (*18*). Thus, Mff punctae may mark the future sites of mitochondrial division before Drp1 recruitment (*18*). In Cos-7 cells transiently transfected with

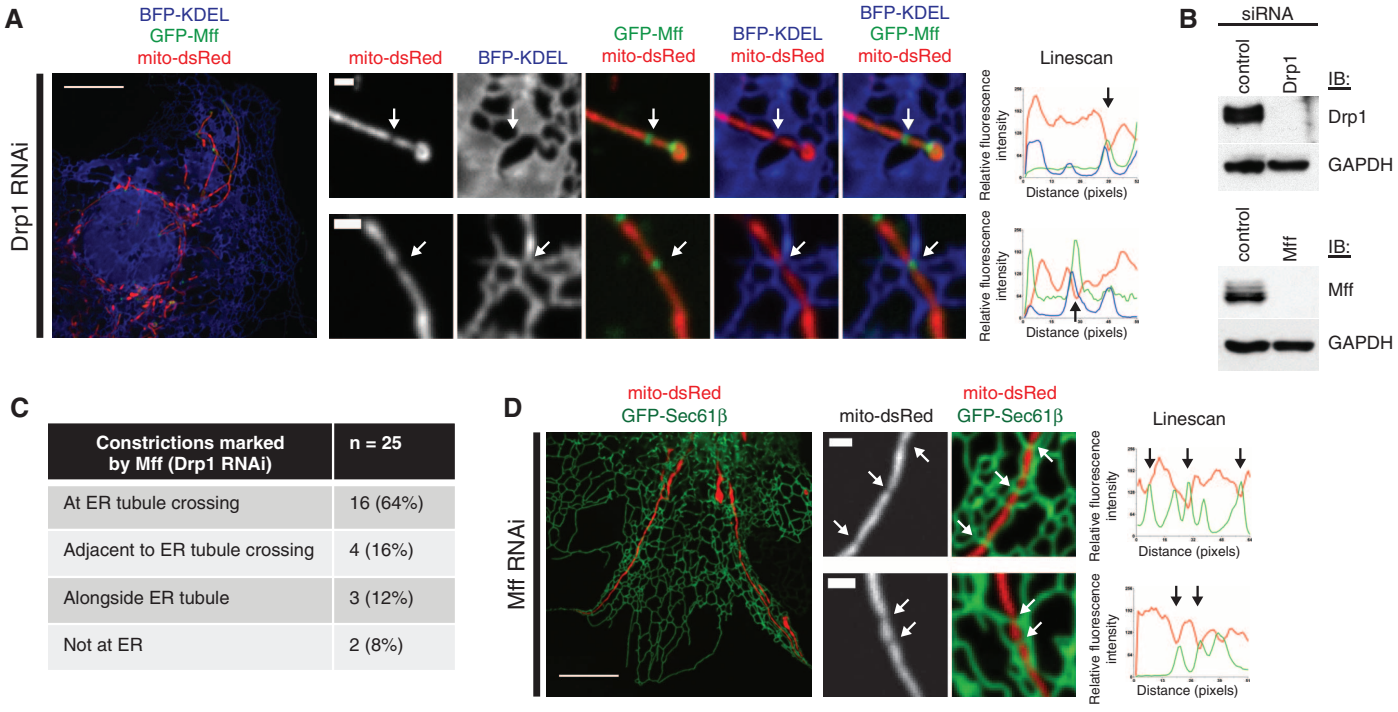

Constrictions marked by Mff (Drp1 RNAi)	n = 25
At ER tubule crossing	16 (64%)
Adjacent to ER tubule crossing	4 (16%)
Alongside ER tubule	3 (12%)
Not at ER	2 (8%)

Fig. 4. The ER localizes to mitochondrial constrictions before Drp1 and Mff recruitment. (**A**) Examples of mitochondrial constrictions at ER contacts marked by Mff in Cos-7 cells depleted of Drp1. Left and center images show these cells expressing mito-dsRed, BFP-KDEL (ER), and GFP-Mff, merged as indicated. Right graphs are line scans drawn through the mitochondria and show the relative fluorescence intensity of mitochondria (red), ER (blue), and Mff (green) along their length. White arrow positions at constrictions correspond to black arrows on the line scan. Additional examples are shown in fig. S6. (**B**) Western blots with antibody against Drp1 (top) or Mff (bottom) and GAPDH demonstrate depletion of Drp1 in lysates from cells transfected with siRNA against Drp1 [as in (A)] or Mff [as in (D)] compared with control RNAi cells. (**C**) The number of Mff-localized mitochondrial constrictions in Drp1-depleted cells that colocalize with ER tubules, from 23 cells. (**D**) As in (A), for cells depleted of Mff and expressing GFP-Sec61β (ER; green on line scan) and mito-dsRed (red on line scan). Scale bars for (A) and (D) large left images, 5 μm; (A) and (D) smaller center images, 1 μm.

GFP-Mff, mCherry-Drp1, and mito-BFP, we observed that Mff circumscribed and localized to punctae on mitochondria, the majority of which colocalized with Drp1 (fig. S5, A to C). To test whether Mff punctae localize to ER contacts independently of Drp1, we depleted Drp1 from Cos-7 cells with small interfering RNA (siRNA) and cotransfected these cells with GFP-Mff, mito-dsRed, and BFP-KDEL (ER). Drp1 was substantially depleted in Drp1 RNA interference (RNAi) cells in comparison with the control cells (Fig. 4B). Selective depletion of Drp1 was further supported by the aberrant and elongated mitochondrial morphology in Drp1 RNAi cells (Fig. 4A and fig. S5D). As expected (*18*), in Drp1-depleted cells, Mff punctae localized to mitochondria (Fig. 4A). We asked whether mitochondria were constricted at Mff punctae in the absence of Drp1, and if so, whether these sites localized to ER contacts. Of the 25 constrictions we resolved, 16 were at an ER crossover (64%), and another 4 were adjacent to an ER tubule crossing (16%) (Fig. 4, A and C, and fig. S6). Thus, Mff localizes in a Drp1-independent manner to mitochondrial constrictions at sites of ER contact. We next asked whether the ER localizes to regions of mitochondrial constriction in the absence of Mff. Cos-7 cells were depleted of Mff by siRNA and cotransfected with GFP-Sec61β (ER) and mito-dsRed. As expected, mitochondrial morphology was elongated in these cells (Fig. 4, B and D, and fig. S5E). In cells depleted of Mff, we observed mitochondrial constriction at sites of ER contact, indicating that ER-mitochondrial contacts form and mark positions of mitochondrial constriction independently of both Mff and Drp1 recruitment (Fig. 4D).

Here, we have shown that ER-mitochondrial contacts are a conserved feature of mitochondrial division. We envision two ways that ER contact might directly regulate mitochondrial division: (i) ER proteins intimately participate in division, and/or (ii) ER tubules physically wrap around and constrict mitochondria to a diameter comparable to Dnm1 and Drp1 helices to facilitate their recruitment and assembly to complete fission (fig. S9). The latter is attractive given that the diameter of Dnm1 helices (~110 to 130 nm) is considerably narrower than that of mitochondria and is quite similar to the diameter of constricted mitochondria at ER tubule contacts (138 nm and 146 nm) (*4*, *6*–*9*). Regardless of the exact mechanism, the ER appears to mark the division site and is likely to be an active participant in this process, because it remains in contact with the mitochondria through the entire fission event. Many human diseases are associated with excessive mitochondrial division, raising the intriguing possibility that these diseases could involve an alteration of ER-mitochondrial contacts.

References and Notes

1. D. H. Cho, T. Nakamura, S. A. Lipton, *Cell. Mol. Life Sci.* **67**, 3435 (2010).
2. Y. Yoon, C. A. Galloway, B. S. Jhun, T. Yu, *Antioxid. Redox Signal.* **14**, 439 (2011).
3. L. L. Lackner, J. M. Nunnari, *Biochim. Biophys. Acta* **1792**, 1138 (2009).
4. E. Ingerman *et al.*, *J. Cell Biol.* **170**, 1021 (2005).
5. S. Gandre-Babbe, A. M. van der Bliek, *Mol. Biol. Cell* **19**, 2402 (2008).
6. A. Legesse-Miller, R. H. Massol, T. Kirchhausen, *Mol. Biol. Cell* **14**, 1953 (2003).
7. A. M. Labrousse, M. D. Zappaterra, D. A. Rube, A. M. van der Bliek, *Mol. Cell* **4**, 815 (1999).
8. Y. Yoon, K. R. Pitts, M. A. McNiven, *Mol. Biol. Cell* **12**, 2894 (2001).
9. J. A. Mears *et al.*, *Nat. Struct. Mol. Biol.* **18**, 20 (2011).
10. O. M. de Brito, L. Scorrano, *EMBO J.* **29**, 2715 (2010).
11. O. M. de Brito, L. Scorrano, *Nature* **456**, 605 (2008).
12. B. Kornmann *et al.*, *Science* **325**, 477 (2009); 10.1126/science.1175088.
13. J. R. Friedman, B. M. Webster, D. N. Mastronarde, K. J. Verhey, G. K. Voeltz, *J. Cell Biol.* **190**, 363 (2010).
14. M. West, N. Zurek, A. Hoenger, G. K. Voeltz, *J. Cell Biol.* **193**, 333 (2011).
15. G. K. Voeltz, W. A. Prinz, Y. Shibata, J. M. Rist, T. A. Rapoport, *Cell* **124**, 573 (2006).
16. H. Sesaki, R. E. Jensen, *J. Cell Biol.* **147**, 699 (1999).
17. E. Smirnova, L. Griparic, D. L. Shurland, A. M. van der Bliek, *Mol. Biol. Cell* **12**, 2245 (2001).
18. H. Otera *et al.*, *J. Cell Biol.* **191**, 1141 (2010).
19. Materials and methods are available as supporting material on *Science* Online.

Acknowledgments: This work is supported by NIH grant R01 GM083977 and a Searle Scholar award (to G.K.V.), NIH training grant GM08759 (to J.R.F.), NIH grant R01 GM062942 and an American Heart Innovative Research Grant (to J.N.), and grants from the Biological Sciences Initiative (BURST grant) and the Undergraduate Research Opportunity Program at the University of Colorado (to J.R.D.). We thank the Boulder 3D Electron Microscopy facility for shared equipment and helpful suggestions.

Supporting Online Material

www.sciencemag.org/cgi/content/full/science.1207385/DC1
Materials and Methods
SOM Text
Figs. S1 to S9
References (*20*–*29*)
Movies S1 to S5

22 April 2011; accepted 17 August 2011
Published online 1 September 2011;
10.1126/science.1207385

Antimicrobial Peptides Keep Insect Endosymbionts Under Control

Frédéric H. Login,[1,2] Séverine Balmand,[1,2] Agnès Vallier,[1,2] Carole Vincent-Monégat,[1,2] Aurélien Vigneron,[1,2] Michèle Weiss-Gayet,[2,3] Didier Rochat,[4] Abdelaziz Heddi[1,2]*

Vertically transmitted endosymbionts persist for millions of years in invertebrates and play an important role in animal evolution. However, the functional basis underlying the maintenance of these long-term resident bacteria is unknown. We report that the weevil coleoptericin-A (ColA) antimicrobial peptide selectively targets endosymbionts within the bacteriocytes and regulates their growth through the inhibition of cell division. Silencing the *colA* gene with RNA interference resulted in a decrease in size of the giant filamentous endosymbionts, which escaped from the bacteriocytes and spread into insect tissues. Although this family of peptides is commonly linked with microbe clearance, this work shows that endosymbiosis benefits from ColA, suggesting that long-term host-symbiont coevolution might have shaped immune effectors for symbiont maintenance.

Cooperative associations between animals and symbiotic bacteria are widespread in nature and common in insects that exploit unusually restricted nutritional resources (*1*). In many insects, intracellular bacteria (endosymbionts) are transmitted vertically and provide nutrient supplementation to their hosts, thereby improving their adaptive traits and their invasive power (*2*–*4*).

However, maintaining the beneficial nature of this long-term relationship requires both the host and the symbiont to constrain adaptive interactions. Genomic and evolutionary data have shown that major deletions and mutations of genes occur in endosymbionts, some of which are involved in bacterial virulence and host tolerance (*5*–*7*). Data on how host immune systems have evolved to tolerate cooperative bacteria remain scarce and are mainly limited to extracellular associations with environmental and/or horizontal symbiont transmission (*8*, *9*).

To protect permanent endosymbionts from the host's systemic immune response, and prevent competition with opportunistic invaders, symbionts are sequestered in bacteria-bearing host cells, called the bacteriocytes, which, in some species, group together to form a bacteriome (*10*). To investigate the immune specificities of bacteriocytes, we have studied associations with *Sitophilus*

[1]INSA-Lyon, INRA, UMR203 BF2I, Biologie Fonctionnelle Insectes et Interactions, F-69621 Villeurbanne, France. [2]Université de Lyon, F-69003 Lyon, France. [3]Université Lyon 1, CNRS UMR5534, Centre de Génétique et de Physiologie Moléculaire et Cellulaire, F-69622 Villeurbanne, France. [4]INRA, Université Pierre et Marie Curie, UMR1272 Physiologie de l'Insecte Signalisation et Communication, F-78026 Versailles, France.

*To whom correspondence should be addressed. E-mail: abdelaziz.heddi@insa-lyon.fr